Senescent Accelerated Prone 8 (SAMP8) Mice as A Model of Age Dependent Neuroinflammation

Andrés Fernández
Instituto de Salud Carlos III
Elena Quintana
Instituto de Salud Carlos III
Patricia Velasco
Instituto de Salud Carlos III
Belén de Andrés
Instituto de Salud Carlos III
Maria Luisa Gaspar
Instituto de Salud Carlos III
Isabel Liste
Instituto de Salud Carlos III
Marcal Vilar
Instituto de Biomedicina de Valencia
Helena Mira
Instituto de Biomedicina de Valencia
Eva Cano (ecano@isciii.es)
Instituto de Salud Carlos III https://orcid.org/0000-0003-2750-6135

Research

Keywords: Aging, brain myeloid cells, microglia, inflammatory cytokines, SAMP8

Posted Date: September 9th, 2020

DOI: https://doi.org/10.21203/rs.3.rs-72160/v1

Version of Record: A version of this preprint was published on March 18th, 2021. See the published version at https://doi.org/10.1186/s12974-021-02104-3.

Abstract

Background: Aging and age related diseases are strong risk factors for the development of neurodegenerative diseases. Neuroinflammation (NIF), as the brain's immune response, plays an important role in aged associated degeneration of central nervous system (CNS). The need of animal models that will allow us to understand and modulate this process is required for the scientific community.

Methods: We have analyzed aging-phenotypical and inflammatory changes of brain myeloid cells (bMyC) in a senescent accelerated prone aged (SAMP8) mouse model, and compared with their resistant to senescence control (SAMR1). We have performed morphometric methods to evaluate the architecture of cellular prolongations and analyzed $Iba1^+$ clustered cells with aging. To analyse specific constant brain areas we have performed stereology measurements of $Iba1^+$ cells in the hippocampal formation. We have isolated bMyC from brain parenchyma (BP) and choroid plexus and meningeal membranes (m/Ch), and analyzed their response to systemic LPS- driven inflammation.

Results: Aged 10 month old SAMP8 mice presents many of the hallmarks of aging-dependent neuroinflammation when compared with their senescence resistant control (SAMR1); ie, increase of protein aggregates, presence of $Iba1^+$ clusters, but not increase in the number of Iba1+ cells. We have further observed and increased of main inflammatory mediator IL-1β, and augment of border $MHCII^+Iba1^+$ cells. Isolated $CD45^+$ bMyC from brain parenchyma (BP) and choroid plexus and meningeal membranes (m/Ch) have been analyzed showing that there is not significant increase of $CD45^+$ from the periphery. Our data support that aged-driven pro-inflammatory cytokine interleukin 1 beta (IL1β) transcription is mainly enhanced in $CD45^+$BP cells. Furthermore, we are showing that LPS-driven systemic inflammation produces inflammatory cytokines mainly in the border bMyC, sensed to a lesser extent by the BP bMyC, and is enhanced in aged SAMP8 compared to control SAMR1.

Conclusion: Our data validate the SAMP8 model to study age-associated neuroinflammatory events, but careful controls for age and strain are required. These animals show morphological changes in their bMyC cell repertoires associated to age, corresponding to an increase in the production of main pro inflammatory cytokines such as IL-1β, which predispose the brain to an enhanced inflammatory response after LPS-systemic challenge.

Background

As life expectancy increases, age and age-related diseases have become a major health concern in western societies. Aging is the strongest risk factor for neurodegenerative diseases and while aging in itself is not considered a disease, it results in important changes in brain tissue: significant increase in glial activation, complement factors and inflammatory mediators with concomitant brain atrophy [1, 2]. Microarray and single-cell RNAseq studies of aged human and mouse brains extended these findings by

showing that genes related to cellular stress and inflammation increase with age while genes related to synaptic function/transport, growth factors, and trophic support decrease [3–6].

A link between aging, neuroinflammation and promotion of neurodegenerative diseases such as Alzheimer disease (AD), Parkinson diseases or vascular associated dementia has been proposed [7]. Neuroinflammation (NIF), defined as the brain's immune response, has been linked to age-associated neurodegeneration (reviewed in [8]). CNS was considered to be isolated and protected from immune responses, but it is now apparent that the blood–brain barrier (BBB) is not impermeable to inflammation and that neuroinflammation occurs in the brain with similar features to inflammation in the periphery. A role for adaptive immune response in the CNS is now accepted (reviewed in [9]; [10]). The main indicators of a primary neuroinflammatory response are phenotypic glial activation and de novo production of immune signalling molecules. Both, astrocytes and microglia undergo cellular hypertrophy with increased expression of cell-surface immune modulatory proteins, including those of the major histocompatibility complex (MHC), changes which are accompanied by increased synthesis and release of pro-inflammatory cytokines and chemokines (reviewed in [11]). Although different type of cells have been involved in this process, the main cell types involved in the CNS inflammation belong to the myeloid cell compartment. Brain myeloid cells (bMyC) comprise mainly microglia cells, and include perivascular, meningeal and choroid plexus macrophages, periphery-derived monocytes, and brain dendritic cells (bDC), with a role in this process [12].

Parenchymal microglia, the often referred to as brain macrophages, are clearly implicated in the steady-state brain and in the response to different brain injuries. They have a myeloid origin; are derived from embryonic yolk sac progenitors and are sustained by local progenitors [13] [14, 15]. One of the hallmarks of age-dependent microglia cells is their morphological changes. Microglia cells in the young normal brain, are cells with long and ramified prolongations [16, 17]. Aged microglia cells have ramified morphologies that are less branched, have shorter overall process lengths, and cover less dendritic “territory” than those of young microglia. Therefore, aged microglia presents a reduced “arborization” [18, 19] and characteristic accumulation in clusters, which might correspond to microglia responding to anomalous brain protein accumulation, stress related processes, or a direct effect of the aging process on the microglia itself (reviewed in [1]; [20, 21]). Furthermore, upon an inflammatory stimulus, these cells pass to an activated phenotype, which is characterized by morphological changes and cytokine synthesis, finally acquiring phagocytic capacity [22]. Morphologically, this activation is characterized by hypertrophy of cell body, widening of proximal processes and reduction of distal branches [23]. Therefore, the observation of changes in microglia cells in particular and bMyC in general, is characteristic of neuroinflammation.

Aging, as a progressive process associated to chronic low-grade inflammation and their neuroinflammatory-associated events has been linked to neurodegenerative diseases [24]. In rodent models of Alzheimer disease (AD), chronic stress exacerbates neurodegeneration and cognitive impairments [25, 26], concomitant with increases of Aβ peptide accumulation and Tau protein phosphorylation modelled in different animal models (reviewed in [27]). In this context, the senescence

accelerated mouse prone 8 (SAMP8) has been proposed as a neurodegeneration model to study Late Onset Alzheimer Disease (LOAD) related to aging [20, 28–30]. This model presents many of the hallmarks found in neurodegenerative processes; impairments in learning tasks, as well as altered emotions and abnormality of the circadian rhythm [31], spongy degeneration [32], neuronal cell loss [33], and gliosis in the brain [34]. Notably, SAMP8 mice also show other characteristics seen in AD patients, such as learning and memory deficits [35], increased Aβ levels [21], impaired neurogenesis [36, 37], activation of microglia, and an unfavourable inflammatory microenvironment [38, 39].The neuroinflammatory state of SAMP8 model has been studied [40–42] but not clearly characterized, and the specific changes that take place in the brain myeloid compartment of these animals remain to be fully explored.

The hallmark of a neuroinflammatory response is phenotypic glial activation and the production of immune signalling molecules such as interleukin-1β (IL-1β). IL-1β is involved in elaboration of acute neuroinflammatory events, and the main cellular source in the brain is microglia (reviewed in [43]). Aged microglia cells are skewed toward a phenotype characterized by increased pro-inflammatory cytokine release, such as IL-1β, tumour necrosis factor-α (TNF-α) and IL-6 [19, 44]. Indeed, persistent microglial pro-inflammatory activation exacerbate neuronal damages and amyloidosis already present in AD pathology [45], and an increase in inflammatory markers have been described in SAMP8 blood plasma [40]. Furthermore, augmented expression of pro-inflammatory cytokines IL-1β, TNF-α and IL-6 in SAMP8 brain tissues has been shown [42].

In this context, it has been described that systemic inflammation has a role in the progression of chronic neurodegenerative diseases. A hallmark of aged microglia is the fact that they are primed by chronic inflammatory environment and, therefore, aged microglia responds more vigorously to a given systemic inflammatory stimuli. This phenomenon was introduced as microglia priming [19, 46, 47]; reviewed in [48]. Innate immunity activates defensive mechanisms within minutes of microbial invasion through pattern recognition receptors (PRRs) such as Toll-like receptors (TLRs). Lipopolysaccharides (LPS), a component of the outer membrane of Gram-negative bacteria, are responsible for the induction of inflammatory conditions, and LPS systemic administration is been used to test immune system activation and the role in neurodegeneration [49]. Thus, higher doses can lead to pathological reactions such as the induction of septic shock, while lower doses of circulating LPS are associated with chronic disease characterized by persistent low-grade inflammation [50]. This inflammatory response involves activation of PRRs and subsequent production of many pro-inflammatory cytokines such as IL-1β, TNF-α or IL-6. We have asked if isolated bMyC from aged senescent SAMP8 recapitulate this enhanced response.

In this work, we have analysed the number and function of bMyC in the senescence SAMP8 model comparing to resistant control strain SAMR1. We have analyzed the morphology and distribution of hippocampal macrophages/microglia ($Iba1^+$) cells by immunohistochemistry. We have quantified the number of hippocampus $Iba1^+$ using stereology methods comparing young (2 months) and aged (10 months) animals from both strains, and isolated and analysed the number of $CD45^+$ cells by cytometry studies. Finally, we have studied the expression of pro-inflammatory cytokines produced by isolated

bMyC from the two main areas in which are abundant: the brain parenchyma (BP) and brain areas in contact with the periphery, meningeal and choroid plexus (m/Ch). We have further evaluated the response to low doses of inflammatory challenge of isolated cells from BP and m/Ch indicating a different activation kinetics of cells from both brains localizations.

Methods

Mice

Adult (2 to 10 months old) SAMP8 and SAMR1 mice were bred and maintained in the animal facilities at the Centro Nacional de Microbiología - Instituto de Salud Carlos III (CNM-ISCIII, Madrid, Spain). Male double transgenic APP/PS1 mice (10 months old), a cross between Tg2576 (overexpressing human APP695) and mutant PS1 (M146L), were kindly provided by Eva Carro [51]. All animal experiments were approved by the Institutional Review Board at the ISCIII and carried out in strict accordance with EU and National Animal Care guidelines. Protocols were approved by Consejería de Medio Ambiente Comunidad de Madrid (PROEX 179-14).

Tissue Processing

For confocal preparations, mice were deeply anesthetized by intraperitoneal (ip) injection of a mixture of ketamine and xylazine and transcardially perfused with 25–30 mL of saline solution for 5 min, followed by 10 min with 4% paraformaldehyde (PFA) from Sigma, pH 7.4, in 0.1 M phosphate buffer (PB, Sigma). After perfusion with the fixative, brains were dissected out and post fixed with 4% PFA for 18–20 h at 4ºC. After fixation, brains were rinsed in 0.1 M PB and placed in 15% glucose at 4ºC until they sank, and then in 30% sucrose in PB at 4ºC for 72 h. Finally, brains were embedded in tissue freezing medium (Tissue-Tek O.C.T^{TM}, Sakura), by submerging brains in increasing concentrations of OCT, frozen immediately in dry-ice-cooled 2-methylbutane (Sigma), and stored at -80ºC. Coronal sections (30 μm) were cut using a CM1950 cryostat (Leica Microsystems). Brain sections were collected sequentially in 10 slides. Six sections per slide generates antero-posterior reconstructions of the hippocampus conformed by 1 section every 300 μm of hippocampal structure and stored at -20ºC until use.

Periodic acid–Schiff (PAS) stain

Frozen brains embedded in OCT cryostat-embedding compound (Tissue-Tek) as before, were cut into 30μm-thick sections on a cryostat (Leica) at −22◦C, and placed on slides. Sections of the central zone of the hippocampus (at about bregma −2.30) were selected according to mouse brain atlas. Brain sections were and hydrate to deionized water and immerse in 0,5% periodic acid for 5 minutes at room temperature (18–26°C). Slides were rinsed in several changes of distilled water and immersed in Schiff's Reagent (Sigma) for 15 to 20 minutes at 4°C. Slides were rinsed in running tap water for 5 minutes. For nuclei staining, slides were counterstained in Hematoxylin Solution, Gill No. 3 (Thermo Fisher), for 90 seconds, rinsed with alcohol acid (0,5% HCl in EtOH) three times and a final rinsed with tap water. Finally, slices were dehydrated, cleared and mounted in DPX (Sigma-Aldrich) media.

Immunohistochemistry

Immunohistochemistry analyses were performed on frozen brain sections by standard indirect staining as in [52]. Antibodies were diluted in 0.1 M PB containing 1% Foetal Bovine serum (FBS) (Hyclone), 0.06% Triton-X100 (Sigma), and 150 mM glycine (Merck). Rabbit anti-Iba1 (1:100, Wako) was used to detect expression of bMyC, Rat anti-mouse I-A/I-E (1:100, clone 2G9, B.D. Pharmingen) was used to detect antigen-presenting cells, Mouse anti-phospho-Ser 139-Histone H2A-X (clon JBW301, Millipore) was used to analyze DNA damage. Alexa fluor 488 Donkey anti-rabbit, -rat, -mouse and Cy3 anti-rat antibodies (Jackson) were used as second antibodies. After staining, all sections and cells were mounted and preserved with 50% Mowiol (Polysciences), 2.5% DABCO (Sigma).

Confocal Microscopy and Analysis.

Images were acquired on a Leica Spectral SP5 confocal microscope. Brain maps were imaged using a 20X INM objective and a 1.7 digital zoom. Tissue images are tiles of 2-4 µm z-stacks and cell images are single 1-2 µm z stacks both captured on a Leica Spectral SP5 confocal microscope with a 40x and 63X oil objectives. Images are presented as average projections of z-stacks and keeping parameters constant using negative control slides stained with primary antibody to identify potential nonspecific, background fluorescence. Exceptions are mentioned in Fig legends. Acquired z-stacks were background-subtracted with Leica LAS AF 2.6.3 software and secondary processed and analyzed using Adobe Photoshop CS3 (Adobe Systems) and ImageJ (National Institute of Health, **http://rsb.info.nih.gov/ij**) for ROI quantification and cell counting. For 3D reconstructions, the plugging 3D viewer for ImageJ was used.

Stereology and Statistical analysis.

Stereology was performed by the analysis of 5 to 6 coronal sections, 30 µm each, separated 300 µm one to each other. Sampling started at first appearance of the infrapyramidal blade of the dentate gyrus (DG). Antero-posterior Bregma coordinates of all 5 sections correspond approximately to -1.2 mm, -1.6 mm, -2 mm, -2,4 mm and -2,8 mm. Every quantification was normalized by the DG area of every section. Analysis of variance (ANOVA) was used for statistical analysis of differences between ages of the same strain. Post-hoc comparisons were performed using the Tukey test, and the Bonferroni correction was applied. Data were also analysed by 2-tailed Student t test (unpaired t test for analysis of both SAMR1 and SAMP8 strains of the same age). Data are presented as mean ± standard error of the mean (SEM) and n indicates the number of independent mice used per strain and age. A p value of <0.05 was considered as statistically significant.

Image analysis for morphometric parameters calculation.

Three-dimensional (*3*D) reconstruction of individual microglial cells Z-stack confocal images of around 30 µm thickness at intervals of 1 µm were taken at specified areas of SAM R1 and P8 brain of different age. 3D images were obtained by using the plugin 3D viewer of FIJI software (freely downloadable from http://fiji.sc/Fiji). To analyse spatial coverage of microglia we used the methods described in Baron et al

2014 modified. Briefly, brain sections from these mice were stained with Iba1, and two distinctive areas of the brain such as the hippocampal formation (Hpp) together with areas within this brain area: strata pyramidale (sp) and oriens (so) imaged with confocal microscopy as before. Then, grey-level maximum z projection images were set to eliminate background based on intensity threshold and converted to binary images, processed with the 'skeletonize' option in FIJI software, and further analysed with a modified Sholl's analysis adapted for microglia as in [18, 53]. A representative heat-map image was generated based on 8-bit z-projection image using the 3D Surface Plot plug-in bundled in FIJI software. For morphometric parameters calculation, after tracing an individual microglial cell, we calculate the number of intersections between microglial processes and concentric circles originated from the center of individual cell we used the Sholl's analysis plug-in (Ghosh Lab, UCSD, San Diego, CA, USA) bundled in FIJI. This was used to analyze the number of intersections in circles with a radius between 5um (*starting radius*) as minimal distance corresponding to the soma of the cell and the final radio which include the longest microglia branch (*ending radius*). We analysed at least 25 individual Iba-1+ cells from a total of three individual animals. We present the data by using polynomial regression and defining three parameters: critical value of the circle radius (which defines the place of a possible circle intersecting maximum number of dendrites); the maximum number of ramification intersections with the circles (counted for consecutive circles placed starting at the cell body to the border of the arborisation and the mean value of the fitted polynomial function (which describes an average property concerning numbers of branches of ramification tree over the whole region occupied by the ramification arbor). For that purpose, we also used the Sholl regression coefficient as well as the Schoenen ramification index similar to that described previously [54, 55].

LPS administration to mice

To assess the response of brain myeloid cells to peripheral immune stimulation, mice received a single intraperitoneal injection (i.p) of LPS from E. coli. #0111:B4; L4391-IMG (Sigma) of 0.5 to 1 mg/kg LPS. The LPS powder was dissolved in 0.9% endotoxin-free sterile saline at a concentration of 10 mg/ml. Mice injected with sterile saline as vehicle were used as control. Brains were collected and cells preparation and mRNA expression analyses as follow.

Cell Preparation

2 and 10 months old SAMP8 and SAMR1 mice (or otherwise specified) were sacrificed, and intracardiac perfusion was performed using phosphate buffered saline (PBS) with observed blanching of the spleen during 5 min at a speed of 5 mL/min. Complete brains were dissected and for most experiments meningeal (piamater) membranes and choroid plexus (m/Ch) were carefully removed with fine tweezers. Brain tissue was finely minced into small pieces and treated with a specific protease mix depending on the tissue. For brain without m/Ch, cells were prepared as in [52], brain, without the m/Ch and cerebellum, was digested in 5 mL of enzyme solution 20 units/mL papain (Worthington) and 0.025 units/mL DNAse (Sigma) in buffer containing 116 mM NaCl, 5.4 mM KCl, 26 mM $NaHCO_3$, 1 mM NaH_2PO_4, 1.5 mM $CaCl_2$, 1 mM MgSO4, 0.5 mM EDTA, 25 mM glucose, and 1 mM l-cysteine, pH 7.5) for 30 min at room

temperature (RT) with agitation. The brain homogenate was washed and filtered once through a 70-μM filter to remove undigested fragments and then washed twice more, followed by centrifugation at 300*g* for 7 min. Cells were resuspended in 30% Percoll (GE Lifesciences) under 5 mL HBSS and centrifuged at 300*g* for 20 min at RT with slow acceleration and no brake. Pellets were collected and washed with ice-cold PBS containing 2% (vol/vol) FBS (spin 300*g*, 7 min). All subsequent washes were performed in this buffer. This preparation contains microglia/macrophage from brain as in [56], with the exception of those from meningeal membrane, choroid plexus, and cerebellum; we refer to this cell preparation as brain myeloid cells (bMyC) fom brain parenchyma (BP). For m/Ch cell isolates, meningeal membranes plus choroid plexus were collected in an Eppendorf containing 1 mL PBS. Tissue was treated with 2.5 mg/mL pronase (Roche) plus 0.025 units/mL DNase (Sigma) in PBS during 30 min at 37°C in a bath with mixing. This was followed by homogenization with gentle trituration using glass pipettes until an even homogenate was obtained. m/Ch homogenates were filtered and treated as above. All subsequent steps were performed at 4°C in PBS, 2% FBS.

CD45+ cell purification

After enrichment on Percoll gradient, brain isolated cells where purified using MACs LS columns from Miltenyi Biotec, following manufactures instructions. Cells were washed in PBS 2% FBS and resuspended in 180 μL of PBS 0.5% BSA 2mM EDTA per brain sample, using MACs solutions, following manufacturer instructions. All steps were carried out on this buffer. CD45 mouse microbeads (20 μL) where added to the cells and incubated on ice during 15 minutes. 5 mL where then added and cell suspension was centrifuged 10 minutes at 300 g. Supernatant was discarded and cells were resuspended in 5 mL and applied to the column, attached to MACs Separator and previously equilibrated with same buffer. Before column, cell preparation were filtered through 70μm filter. Column was washed with 10 mL and cells where extracted from column in 5 mL according to Miltenyi protocol. Cells were centrifuged again and resuspended in 1 mL of PBS-Serum, counted in a Neubauer chamber and prepared for following applications.

Flow Cytometry

Single-cell suspensions were prepared as above and resuspended in staining buffer (2.5% FBS in Dulbecco's PBS; Biowhittaker, Lonza Group). Nonspecific binding to Fcγ receptors was blocked with 10 μg/mL of 2.4G2 mAb (Fc block) (BD Biosciences). Staining was performed following standard protocols. Antibodies and reagents are listed in Supporting Information, Table 1. Fluorochrome-labeled antibodies specific for mouse CD45, CD11b, P2RY12 and CD49d were from BD Biosciences or Biolegend. Cells were analyzed on a LRS Fortessa X-20 (BD Biosciences) cytometer, using the FlowJo v6.3.4 (TreeStar) and DIVA v8.0 software packages. The gating strategy used to exclude dead cells and doublets is presented in aditional Fig 2s

RNA isolation and Real-Time PCR

Total RNA was extracted with Tripure (Roche), and 2 µg were reverse transcribed to cDNA with MMLV-RT (Invitrogen). Real-time quantitative PCR (qPCR) was carried out on 10-20 ng cDNA, using TaqMan probes and Sybr Green system (Applied Biosystems). qPCR reactions were run in duplicate in ABI Prism 7500 Fast Sequence Detection System (Applied Biosystems). Mouse primers used for Sybr Green assays were as follow, 36B4 was used as endogenous control.

36b4 Forward: AGATGCAGCAGATCCGCAT

Reverse: GTTCTTGCCCATCAGCACC

Il-1β: Forward: CAACCAACAAGTGATATTCTCCATG

Reverse: GATCCACACTCTCCAGCTGCA

Tnf-α Forward: TGGAACTGGCAGAAGAG

Reverse: CCATAGAACTGATGAGAGG

Il-6: Forward: GAGGATACCACTCCCAACAGACC

Reverse: AAGTGCATCATCGTTGTTCATACA

Ccl-2: Forward: CGGAACCAAATGAGATCAGAACCTAC

Reverse: GCTTCAGATTTACGGGTCAACTTCAC

Aif-1: Forward: GGGAAAGTCAGCCAGTCCT

Reverse: GCATCACTTCCACATCAGCTT

Cx3cr1 Forward: TCAGCATCGACCGGTACCTT

Reverse: CTGCACTGTCCGGTTGTTCA

Results

Hippocampal PAS positive granules are increased in aged SAMP8

As has been previously stated the presence of granular accumulation is a hallmark of the neurodegenerative associated process in human brain [57], and aged animals [58] and. These accumulations are often referred as periodic acid-Schiff (PAS) positive granules. The nature of these granules in different mouse strains is still under discussion. PAS positive granules have been observed in the hippocampus and entorhinal cortex of a variety of different species and associated to aging in senescent accelerated prone 8 (SAMP8) animal model (reviewed in [59]). To localize a valid area of the brain in which neurodegenerative-associated processes are taking place, we analyzed 2 months (2 m)

and aged 10 m old animals from the SAMP8 strain and their control senescent resistant-1 (SAMR1) mouse strain. First, we evaluated 30 m sliced from 10 m SAMP8 brains (from olfactory bulb to cerebellum), stained with PAS (pink staining) and nuclei were counter-stained with haematoxylin (blue-brown). PAS positive granules were observed mainly in hippocampal and entorhinal areas as described [60], although a clear staining in blood vessels was observed (data not shown). The hippocampus (Hpp) in this study refers to the *dentate gyrus* (DG) and the *cornu ammonis 1* (CA1) area of hippocampus proper. We also evaluated the Hpp of 10 m old SAMR1 as non-senescent control, and aged 10 m transgenic APP-PS1 animals as neurodegeneration-associated control. As shown in Fig 1, a very clear increase of PAS positive granules were observed in 10 m old P8 brains, compared to 10 m SAMR1, in numbers that were comparable with those obtained in 10 m old APP-PS1 transgenic animals. The presence of these aged-associated protein accumulations indicate that the brain hippocampus is a suitable area to study the neurodegeneration associated neuroinflammation derived events that take place.

Iba1$^+$ cells from aged SAMP8 mice present clear morphological changes.

Microglial morphology is altered in the cortex of aged human [2] and old mice [18]. Therefore, we aimed to study the complexity of microglia processes with age in SAMP8. We took serial z-stack images and traced the backbone of cells throughout the z-stack images with the FIJI software as specified in Material and Methods and as in [18]. We performed Sholl analysis as a morphometric method that evaluates the architecture of cellular prolongations; these analyses draw a series of concentric circles around the cell soma, and consists in a mathematical method that gives a measure of the prolongation arborization that can be used to study microglia ramifications [61, 62]. First, we obtained the number of primary ramifications as the number of extension originated in the cellular body or soma, and the Schoenen ramification index (SRI), described as the ratio between the maximum number of the intersections of microglia ramifications with the circles and the number of the primary ramifications. Our analyses show that 2 m old SAMP8 Hpp presented a lesser arborization index than their 2 m old Hpp SAMR1 controls. In contrast, 10 m old SAMP8 Hpp Iba1$^+$ cells have similar number of primary ramifications than their 10 months SAMR1 counterparts, although significant changes in their ramification index were observed (Fig 2). Therefore, we conclude that Iba1$^+$ cells in aged SAMP8 animals present morphological changes similar to those described in normal aging [18, 63]. Furthermore, aged SAMP8 Iba1$^+$ cells occupied smaller territories, and they displayed more irregular processes than control animals.

Clustered Iba1+ cells are increased in aged SAMP8 and do not express specific markers for DNA damage (HA2X), nor activation related marker such as MHCII.

Another age-dependent microglia morphological change is the appearance of dystrophic microglia and cellular clusters [64, 65]. Therefore, we analyzed the number of very apparent Iba1$^+$ clusters (defined as multinucleated or joined cells) in SAMP8 and SAMR1 brains at different age. We chose two representative brain areas: the stratum oriens in the Hpp and the Thalamus. Iba1$^+$ clusters were hardly present in 2 m SAMR1 brains as control, and were noticeable in 2 m old SAMP8 brains mainly in the Hpp

but not in the Thalamus. When 10 m old P8 brains were studied, Iba1$^+$ clusters were very prominent in both brains areas (Fig 3). The origin of these cellular clusters is unknown, and we hypothesize that might be due to cellular aging and associated DNA damage. DNA damage, whether it is endogenous or exogenous, forms double stranded breaks (DSBs) a phenomena that is followed by the phosphorylation of the histone gamma H2AX (γHA2X$^+$) [66]. Furthermore, expression of γHA2X$^+$ cells has been used as a cellular senescence marker [67]. We evaluated the number of γHA2X$^+$ cells in 10 m old SAMP8 animals, focusing on Iba1$^+$cells. We found γHA2X$^+$ cells in aged 10 m SAMP8 brains, but most of these cells do not express the Iba1 marker. The number of double positive γHA2X$^+$ Iba1$^+$cells in the cellular clusters was very low (< of 0,1± 0,01%). These results indicate that clustered Iba1+ cells do not specifically present associated DNA damage events, and may be functional microglia.

Microglia cells represent the main antigen-presenting cell (APC) inside the BP during neurodegeneration. While expression of MHCII is low in homeostatic conditions in the brain, it can be rapidly upregulated on bMyC and is used as a marker of their activation [68]. We asked if Iba1$^+$clusters observed in 10 m SAMP8 brains were in fact activated microglia described as Iba1$^+$MHC$^+$ cells. Our analyses showed that these Iba1$^+$ clusters were negative for MHCII, although there was a clear increase of Iba1$^+$ MHC$^+$ cells staining in the choroid plexus of aged SAMP8 compared with young 2 m SAMP8 brains, indicating that there is not an increase in the MHCII$^+$ cells in aged BP SAMP8 microglia (additional Fig 1S).

Number of hippocampal Iba1+ cells differ between aged senescent and control mouse strains.

It has been described that the aging process might affect the number of Iba1$^+$ cells in the brain [69] and in particular in the hippocampus. These analyses have been performed as well in aged SAMP8 mice, in which an increase in CD11b staining has been described in this area [70]. We have analyzed if our animals recapitulate this characteristic feature. To analyze a specific constant brain area between different strains and age samples, we chose to perform stereology measurements as specified in material and methods. Briefly, we performed analysis of 4-5 coronal separated 300 µm one to each other from young (2 m) and elderly animals (10 m), slices were stained with anti-Iba1 antibodies and numbers of Iba1$^+$ cells were evaluated. The hippocampus (Hpp): DG and CA1 areas, as specified in Fig 4A, was analyzed. Surprisingly, but very reproducible, immunohistochemical analyses of total Iba1$^+$ cells in 2 m SAMP8 Hpp showed a significant reduction of Iba1$^+$ cells compared to 2 m old SAMR1 control brains. This decrease in Iba1$^+$ cells was further observed in 10 m old SAMP8 brains, when compared with their 10 m SAMR1 controls (Fig 4B). Therefore, these strains differences complicated further the comparison between aged SAMP8 mice versus SAMR1 mice. To eliminate the “strain factor¨, we evaluated and compared the fold increase of Iba1+ cells of aged (10 m) versus (2 m) in each of the strains. As shown in Fig 4C, our results in Hpp (CA1+DG), indicate that there are not clear differences in Iba1$^+$ cells with age, even in 10 m old SAMP8 animals that show clear phenotypical changes associated to age reviewed in [20] and data not shown.

A way to assess the number of bMyC present in the brain is by isolating brain cells follow by cytometry analyses of the different existing cellular populations. bMyC are the major player in inflammation and they are characterized by the expression of hematopoietic marker such as CD45 and myeloid marker such as CD11b (see introduction). We isolated 2 m and 10 m old SAMP8 and control SAMR1 brain parenchymal cells without the meningeal and plexus membranes (BP) cells by using 30% percoll gradient and analysed the number of CD45+ isolated per brain as shown in Fig 5A. The number of isolated $CD45^+$ bMyC do not significantly change between 10 m aged SAMR1 (48 ± 8%) and SAMP8 (43 ± 10%) n=10. The majority of these cells expressed the CD11b marker for myeloid cells (94,2 ± 2%) n=10, and they further expressed specific markers for microglia such as P2RY12 as shown in Fig 5. There is a clear discrepancy about the difference observed between $Iba1^+$ inmunohistochemical analysis (Fig 4) and CD45+ cells cytometry analyses (Fig 5). Therefore, to clarify this, we evaluated the expression of Iba1 mRNA transcripts in both strains at the different age analysed and observed that in fact, there is a clear decrease in the expression of *Aif1* gene encoding Iba1 in 2 m SAMP8 animals in accordance with the results obtained in the immunofluorescence analyses (Fig 4). To asses if there is in fact less Iba1+ cells, we evaluated the expression of a very different molecule, that has been previously shown is expressed mainly in microglia cells in the brain, the fractalkine receptor (CX3CR1) [71]. In this case, the amount of specific *Cx3cr1* transcript present in all the groups analysed differ only slightly (additional Fig 3s). This indicates that the number of BP microglia cells do not change greatly although there is a clear decrease in the expression of Iba 1 gen (*Aif-1*) that should be further studied. Since we have not found significant aged-associated changes in the number of $Iba1^+$ between aged 10 m SAMR1 and SAMP8 by immunofluorescence analyses, together with the fact that $CD45^+$ isolated cells from 10 m SAMP8 BP do not show significant difference from 10 m SAMR1 control, we concluded that the number of BP bMyC in the SAMP8 brain do not change with age. Furthermore, we suggest that the isolation and evaluation of isolated $CD45^+$ BP cells is the method of choice to analyse differences between different mice strains and conditions.

Number of BP peripheral CD45 high cells increases in aged senescent SAMP8 mice

Immunosurveillance takes place in the central nervous system (CNS) in spite of its specific anatomic features conferring a certain degree of isolation from the periphery [72]. The blood-brain barrier (BBB) prevents free trafficking across the brain vasculature but immune cells can cross the endothelium of post-capillary venules or reach the brain through the choroid plexus and the leptomeninges (mCh) under inflammatory conditions. It has been described that aged SAMP8 animal present a damaged BBB permeable to different molecules [73]. We wanted to analyse if there was an increase in the number of $CD45^+$ from the periphery. First, we used CD45 expression to distinguish proper microglia, which have a medium expression of CD45 ($CD45^m$), and myeloid cells from the periphery as CD45 high ($CD45^h$) [56, 74], and analyzed the number of $CD45^h$ present in the BP from senescent SAMP8 and their SAMR1 control. As shown in Fig 5B, the number of $CD45^h$ increase very slightly in 10 m SAMP8 BP (4,2 ± 1,4%) compared to their 10 m SAMR1 control (3,4 ± 1,4%). The number of $CD45^h$ in aged R1 were not significant higher to their 2m SAMR1 controls or that observed in young 2 m control strains [52].

Therefore, although the amount of $CD45^h$ present in aged senescent animals was slightly higher, the small number of cells is not consistent with a substantial breach of the BBB but with higher permeability of the barrier in old SAMP8 brains, which allow the recruitment of extra numbers of peripheral cells. Cerebral invasion of lymphocytes crucially depends on the interaction of the leukocyte very late antigen-4 (VLA-4) with vascular cell adhesion molecule-1 (VCAM-1) on endothelial cells [75, 76]. VLA-4 (integrin alpha4beta1) is an integrin heterodimer consisting of an alpha chain (integrin α4 = CD49d) and a beta chain (CD29). Therefore, the expression of CD49d has been used to mark brain myeloid cells originated in the periphery [77]. $CD45^h$ cells in our cellular BP preparation were CD3 negative (data not shown) but mainly positive for CD49d (Fig 5B).

Inflammatory profile in isolated brain myeloid cells.

As mentioned before, a characteristic of neuroinflammation is phenotypic glial activation and de novo production of immune signalling molecules. Both astrocytes and microglia undergo cellular hypertrophy with age, and it has been shown that pro-inflammatory cytokines levels increase in the elderly subjects [18, 22, 78]. IL-1β is intimately involved in elaboration of acute neuroinflammatory processes in vivo, and exposure of the rodent brain to IL-1β elicits rapid, robust activation of both astrocytes and microglia. In the senescent model SAMP8, an increase of inflammatory markers has been described in blood plasma and total brain tissue [42]. Therefore, we asked if a source of IL-1β in this model was in fact the brain myeloid cells (bMyC) cellular compartment, since they constitute the main cell type involved in the brain inflammatory process. We analysed *Il1β* expression in $CD45^+$ bMyC preparations from BP (panel A) and from the border-associated myeloid cells contained in the m/Ch preparations (panel B). *Il1β* transcripts from 2 and 10 m old SAMP8 and SAMR1 cellular preparations were analysed by quantitative RT-PCR (qRT-PCR) as described in material and methods. As shown in Fig 6, *Il1β* mRNA expression was significantly higher in BP preparations from aged 10 m old SAMP8 when compared with 10 m old SAMR1. Transcripts expression is shown as delta Ct (dCt) as the Ct of the specific transcript minus *36b4* Ct as housekeeping control. When bMyC from brains border (mCh) were analysed for *Il1β* expression we could not detect any significant changes between groups, indicating that myeloid cells from these brain areas do not seem to contribute to the higher expression of this pro-inflammatory cytokine observed in aged brain SAMP8 (Fig 6B). In fact, *Il1β* transcripts were hardly detected in m/Ch when compared with BP cellular preparations.

Augment of *Il1β* parenchymal expression in brain rodent might increase expression of other pro-inflammatory cytokines, leukocyte chemotactic chemokines, cell surface adhesion molecules, cyclooxygenases and matrix metalloproteases within the brain parenchyma. We analysed in our experimental groups the expression of pro-inflammatory cytokines such as tumour necrosis factor-alpha (TNF-α) and interleukin 6 (IL-6). Furthermore, IL-1β elevations have been implicated in trafficking of peripheral immune cells to the brain mediated by cytokines such as CCL-2 expression (Ref reviewed in [8], therefore we included the expression of this cytokine in our analyses. As shown in additional Fig 4s, *Tnf-α*, *Il-6*, and *Ccl2* mRNA expression was significantly diminished in young (2 m) SAMP8 BP cellular preparations compared to 2 m old SAMR1 similar to the data obtained for *Il1β*. Although mRNA values of

these cytokines were disperse in 10 m old animals, an increase of *Il1β* was observed in BP from SAMP8 aged animals (represented as a lower dCt: Ct_{gene}- Ct_{36b4}). When m/Ch preparations were analyzed, there were not significant changes in the expression of these markers between all the groups tested. We noticed that the expression of m/Ch cytokines were very low for all the pro-inflammatory markers and lower than in BP preparations comparing relative quantification. Thus, these results indicate that aged SAMP8 bMyC express higher mRNAs levels of pro-inflammatory markers mainly in the brain parenchyma and not in border bMyC from m/Ch membranes. Consistent with these data, we have not detected a significant increase in systemic inflammation in 10 m SAMP8 animals, since our preliminary analyses do not detect an increase in inflammatory marker in the blood plasma of these animals (data not shown).

Response to inflammatory stimuli in the senescent model.

The use of lipopolysaccharide (LPS) as a robust systemic inflammogen has been widely described (see introduction). For these experiments we selected a low dose of LPS (i.p. injection 0,5 to 1mg/kg) that does not cause mouse lethality and only induces a limited inflammatory response [79, 80]. While high doses of LPS produce immune activation and lethality characteristic of septic shock, low doses such as the one selected in our study reproduce the chronic inflammation status found in many neurological diseases. Furthermore, the use of this compound has been used to test a phenomenon called “priming” of the aged innate immune response (see introduction). We analyzed if old SAMP8 brains recapitulate this phenotype characteristic of brain aging.

First, we evoked systemic inflammation by LPS and analyzed the expression of *Il-1β,Tnf-α, Il6 and Ccl2* mRNAs at different times, to define the time window for the expression of pro-inflammatory markers in our brain cellular preparation. In accordance with literature, after 3 hours LPS (1mg/kg) intraperitoneal injection brain tissue and isolated bMyC expressed high levels of all these pro-inflammatory markers [19, 81]. We evaluated the expression of these molecules in cellular preparation from BP and from border-associated m/Ch cells. As shown in Fig 7, expression of these molecules was greatly enhanced by LPS in BP although as expected, maximal LPS-dependent transcription of these cytokines was observed in border-associated cells (m/Ch). The expression kinetic was as well faster in m/Ch than in BP cells as correspond to a systemic model of infection.

Once that we have established the time and dose of inflammogen, and the fact that systemic LPS was sensed by the BP cells inducing the expression of pro-inflammatory markers, we analyzed the inflammatory state in bMyC cell preparation as before. Senescent 10 m old SAMP8 and control SAMR1 were injected with saline solution (ss) and LPS (as in material and methods), and after three hours, BP and m/Ch cells were isolated. Levels of inflammatory markers were analyzed as previously described. As shown in Fig 7, LPS induced all the pro-inflammatory markers expression studied in both animal strains, represented as dCt: Ct_{gene}- Ct_{36b4} to visualize the high expression of these genes related to the housekeeping gene *36B4.* It was noticeable that only the *Il-1β* expression was significant higher in aged LPS-challenged SAMP8 animal compared to their control LPS-SAMR1. This phenomenon agrees to

previous results in which there is an age-dependent priming of microglia from aged brains [19, 49], which we show is recapitulated in aged SAMP8 animals.

Discussion

SAMP8 as a model of neurodegeneration associated neuroinflammation

Brain ageing in mice and humans leads to morphological and functional changes that are considered a result of dysfunctional processes. One of these morphological changes is the appearance of pathological granular structures in the hippocampus and their progressive expansion with age [82]. These anomalous PAS positive aggregates have been described in aged SAMP8 mouse, and their nature discussed and reviewed in [57, 59]). Although SAMP8 animals have been proposed as a model for age associated neurodegenerative disease such as Late Onset Alzheimer disease (LOAD) (reviewed in [20]); the brain myeloid cells repertoire in the SAMP8 model has not been fully described. Early findings by Takeda´s group described the presence of accumulation of $CD45^{+}CD11b^{+}$ cells by inmunohistochemical analyses in the CA1 region of the hippocampus in SAMP8 mice [70], concluding that there was an increase in microglia proliferation and the appearance of reactive/activated microglia as cells with thick and short processes and strong staining of CD11b. The effect of aging alone in the number of microglia cell is controversial in the literature. Some authors do not observe an increase of microglia cells in the rat and male mice aged hippocampus [83–85]; other authors found that the number of microglia cell is decreased in the aged hippocampal area [86, 87], or an increase when female animals are analyzed [83]. These discrepancies might be due to different mouse strains, animal age or the fact that different markers for microglia detection and their methods are used. A careful comparison of all these results awaits further analyses. In most of the studies Iba1 staining has been used as a marker for microglia identity/activation, and Iba1 increased expression has been further reported in aged CA1 rat by Immunoblot analyses [84]. Therefore, here we have re-analysed changes in the number and morphology of $Iba1^{+}$ cells associated to senescent-related processes in the SAMP8 brain. Our results here did not support an age-dependent increase of microglia cells in aged SAMP8 brain by two ways. First, the evaluation of the number of BP $Iba1^{+}$ cells by immunofluorescence using stereology mapping of the Hpp, that avoided the examination of different areas or different brain coordinates between samples from a variety of mouse strains and age. Second, the evaluation of the number of isolated $CD45^{+}$ in aged SAMP8 animals compared to their 10 m old SAMR1 control (as shown in Fig. 5). Our studies concluded that, at the age evaluated (10 m), there is not a significant increase of hippocampal $Iba1^{+}$ cells in the old senescent animal SAMP8 with clear hallmarks compatible with brain degeneration, compared to their 10 m SAMR1 control by measuring the expression of $Iba1^{+}$ cells/mm^{2} in each strain. We clearly observed that young 2 m old SAMP8 presents less amount of Hpp $Iba1^{+}$ staining when compared to their SAMR1 controls, which make difficult the comparison between strains. Therefore, to analyze the effect of age between strains we evaluate the fold increase between 2 m and 10 m samples, and reach to the conclusion that there is not increase in the number of Iba1 expression in the aged senescent mice with respect to their control (Fig. 4). The meaning and final outcome of this reduction of $Iba1^{+}$ staining in the

young SAMP8 mice remains to be fully investigated. One possibility to reconcile our observation to those previously reported, in which they observed an increase in the microglia numbers with age, could be the use of older animals (12 m old) that might account for the difference in number of Iba1^{+} cells observed, although not significantly differences at 10 m were observed (Fig. 4). Microglia/CD11b^{+} increase has also been described in response to aging in the SAMP8, a process that is concomitant to age-dependent changes in BBB [88], we have not been able to see such an increase nor proliferation in the BP (Iba1^{+}Ki67^{+} cells) by immunofluorescence (data not shown). Furthermore, we could not detect significant changes in the number of CD45^{+} isolated from these mice (Fig. 5A), nor a substantial increase in the amount of BP CD45^{h} cells from the periphery when compared 10 m old SAMP8 with their SAMR1 controls (Fig. 5B). These analyses are an experimental challenge since they required a careful manual dissection of meningeal membranes (mainly piamater) and choroid plexus, which contained CD45^{h} cells. The novel description of cellular markers that differentiate proper CD45^{+} brain cells from those of peripheral origin will clearly help to stablish the permeability capacity of immune cells with aging.

The activation state of old SAMP8 microglia can be studied by the expression of class 2 major histocompatibility complex molecules (MHCII). MHCII expression is required to establish a robust adaptive immunity in the brain and periphery. The entry and activation of T cells in the brain parenchyma requires a preexisting interaction of these cells with antigen presenting cells (APC). In non-injured young brains, the expression of MHCII is low and mainly restricted to perivascular spaces and border associated macrophages in m/Ch [52, 89]. During the process of aging, a strong increase in brain MHCII^{+} cells has been described in different animal models [90–93]. We evaluated the presence of Iba1^{+}MHCII^{+} cells by immunofluorescence analyses in 10 m aged SAMP8 brains (additional Fig. 1s). MHCII + cells in the BP of young 2 m SAMP8 were hardly detectable, and 10 m old SAMP8 animals do not express higher amount of Iba1^{+}MHCII^{+} cells in BP compared to their young 2 m SAMP8 control. This expression was very low, hardly detectable and restricted to perivascular areas as seen in control animals [52]. We found a clear increase in Iba1^{+}MHCII^{+} cells in the brain border (m/Ch) of 10 m SAMP8 compared to their 2 m controls. We show our analyses in the choroid plexus (additional Fig. 1s), that show the antibody specificity. The existence of this MHCII^{+} cells areas in contact with the peripheral environment might account for priming of these cellular compartment when challenged with systemic LPS. The presence of MHCII specifically of majority of microglia cells in the aged brain as shown in [94] remains controversial. Our data suggest that BP MHCII^{+} Iba1^{+} cells are a minority and the expression of this activation marker is mainly at the Iba1^{+} of border areas m/Ch in the aged SAMP8 mouse. When 10 m aged control mouse strain such as CD1 was analysed, we could not observed an increase in the number of Iba1^{+}MHCII^{+} at 10 m old animals (data not shown). These experiments could not been performed in SAMR1 mice, since the antibody used for these analyses did not recognize the specific haplotype of the SAMR1 animals (H-2Ks) [95].

We isolated cells from two of the main bMyC enriched areas: BP and m/Ch as described [52]. Removal of myelin and cell debris after tissue digestion is a critical step for isolation and purification of brain cells for flow cytometry analysis. Percoll density gradients have been widely used for brain immune cells isolation

[96, 97]. Different density gradients such as 30% [98–100] and 30–70% [19, 96, 101] has been used. In our hands, 30% Percoll media produce more than three-fold increase in the total cell recovery with a better viability. To achieve purity we use magnetic-beads based affinity purification (MACS) with a yield of 97%± 2 (n = 10) $CD45^+$ positive cells. BP preparation will formally contain proper microglia cells, perivascular macrophages and blood-derived macrophages that might infiltrate the CNS and contribute to the pathological sequelae. The hippocampus is an irrigated brain tissue, and since changes in BBB permeability has been reported in the SAMP8 [73, 102]; it is possible that peripheral myeloid cells enter the aged SAMP8 brain. As described in Fig. 5, our BP preparations in the most inflammatory conditions (10 m aged SAMP8 animals) contained mainly proper microglia cells with a medium CD45 expression as described before, therefore, we concluded that the permeability to peripheral lymphocytes of aged SAMP8 mouse BBB is not enhanced compared to aged control SAMR1 animals nor to young animals (data not shown).

Increased levels of pro-inflammatory cytokines such as IL-1β, TNF-α and IL-6 in the aged CNS has been described before [18, 19, 78, 103, 104]. Here, we have studied mRNA expression of these cytokines in bMyC-enriched preparation of SAMP8 and SAMR1 from BP and m/Ch with age. Our data in the aged senescent model are consistent with the increment of inflammatory markers seen in aged brain tissue and aged isolated brain cells as in introduction.

Since IL-1β is intimately involved in elaboration of acute and chronic neuroinflammatory processes in vivo (revised in [43]), here we show that Il1β expression is greatly enhanced in aged SAMP8 bMyC from BP but not in m/Ch (Fig. 6). These results are in accordance to preliminary data indicating that systemic pro-inflammatory markers in aged 10 m SAMP8 animals do not differ greatly from 2 m or their 10 m SAMR1 control (data not shown). Parenchymal expression of IL-1β in rodents increases expression of pro-inflammatory cytokines and leukocyte chemotactic chemokines within the brain parenchyma [43, 105]. Importantly, IL-1β is capable of triggering further increases in its own expression as evidenced by murine IL-1β induction following human IL-1β administration or expression in the brain [43, 106]. Therefore, an increment on the amount of IL1β expression will lead to a neuroinflammatory cascade that it is restricted to the brain tissue in absence of systemic challenges.

We have evaluated further bMyC response to low LPS dose simulating mild inflammatory conditions and not septic shock. The LPS dose used in our experiments (0,5 to 1 mg/kg) is far from the LD_{50} for LPS in mice (5–15 mg/kg) and did not cause significant lethality [79, 80]. Despite this low dose, BP bMyC are able to sense this inflammogen and produce LPS-dependent cytokine increase, indicating that the BBB protected microglia cells are able to sense systemic inflammatory conditions. These data are in accordance of recent data indicating that the entire brain exhibited the ability to respond to endotoxemia provoked by LPS producing a wide repertoire of cytokines [107]. The fact that aging dependent BBB permeability allows the entrance of peripheral immune in the SAMP8 model could play a role in the amplification of neuroinflammation processes in response to systemic inflammation and how to manipulate this entrance will be the focus of future research effort.

Conclusions

Neuroinflammation (NIF) plays an important role in aged associated degeneration of central nervous system (CNS). Here we analyzed the brain myeloid cells repertoire in the senescent accelerated prone aged (SAMP8) mouse model and propose this mouse model to study age-associated neuroinflammatory events. Although aged hippocampal areas from SAMP8 animals do not show clear differences in the number of $Iba1^+$ cells or with age, there are clear phenotypical changes associated to aging and an increment of bMyC inflammatory markers, together with a role in the amplification of the neuroinflammation processes in response to systemic inflammation. The need of experimental models to analyse the role of neuroinflammatory processes in the neurodegeneration associated to aging, open the possibility to study the response of SAMP8 to novel therapeutic approaches.

List Of Abbreviations

CNS
central nervous system; **NIF**:neuroinflammation; **AD**:Alzheimer disease; **bMyC**:brain myeloid cells; **BP**:brain parenchyma; **m/Ch**:meningeal membranes and choroid plexus; **BBB**:Brain blood Barrier; **Iba1**:ionized calcium-binding adapter molecule 1; **bDC**:brain dendritic cells; **MHC**:major histocompatibility complex; **TLR**:Toll-like receptors; **LPS**:lipopolysacharides; **FC**:flow cytometry; **IF**:immunofluorescence; **MACS**:magnetic-beads based affinity purification; **FBS**:foetal bovine serum; **PB**:Phosphate buffer; **PBS**:phosphate buffer saline; **SS**:serum saline; **PFA**:paraformaldehyde; **DAPI**:4 ',6-diamino-2-fenilindol.

Declarations

Ethics Approval and consent to participate: This study was carried out in accordance with EU and National Animal Care guidelines (directive 2010/63/EU and RD 53/2013). All the procedures were approved by the Institutional Review Board at the ISCIII and the “Consejería de Medio Ambiente del la Comunidad de Madrid” (PROEX179/14).

Consent for Publication: “Not applicable”

Availability of data and materials. The datasets generated for this study are available on request to the corresponding author.

Competing interests. Authors declare that they have no competing interests.

Funding: This work was supported by grant from the Spanish Ministry (MINECO) (SAF2016-76451) to E.C.

Authors' contributions. AF, EQ and PV performed experiments, contributed substantially to the analysis and interpretation of the data, and reviewed the manuscript. BdA helped with the flow cytometry experiments. BdA, MLG, HM, MV and IL made substantial contributions to the analysis and interpretation of the data, and critically reviewed the manuscript. EC designed the experimental procedures, made

substantial contributions to the analysis and interpretation of the data, drafted and reviewed the manuscript. Project administration and funding by E.C.

Acknowledgements. We thank Eva Carro (Servicio de Neurología-Neurofisiología Hospital 12 de Octubre, Madrid) for providing APP/PS1 mice; Dr Fernando González-Camacho when at the confocal microscopy for excellent technical assistance and Oscar Zaragoza for technical advice in confocal experimental design.

References

1. Conde JR, Streit WJ. Microglia in the aging brain. J Neuropathol Exp Neurol. 2006;65:199–203.
2. Streit WJ, Sammons NW, Kuhns AJ, Sparks DL. Dystrophic microglia in the aging human brain. Glia. 2004;45:208–12.
3. Lee CK, Weindruch R, Prolla TA. Gene-expression profile of the ageing brain in mice. Nat Genet. 2000;25:294–7.
4. Lu T, Pan Y, Kao SY, Li C, Kohane I, Chan J, et al. Gene regulation and DNA damage in the ageing human brain. Nature. 2004;429:883–91.
5. Ximerakis M, Lipnick SL, Innes BT, Simmons SK, Adiconis X, Dionne D, et al. Single-cell transcriptomic profiling of the aging mouse brain. Nat Neurosci. 2019;22:1696–708.
6. Zhan L, Krabbe G, Du F, Jones I, Reichert MC, Telpoukhovskaia M, et al. Proximal recolonization by self-renewing microglia re-establishes microglial homeostasis in the adult mouse brain. PLoS Biol. 2019;17:e3000134.
7. Frank-Cannon TC, Alto LT, McAlpine FE, Tansey MG. Does neuroinflammation fan the flame in neurodegenerative diseases? Mol Neurodegener. 2009;4:47.
8. Ransohoff RM. How neuroinflammation contributes to neurodegeneration. Science. 2016;353:777–83.
9. Hickey WF. Basic principles of immunological surveillance of the normal central nervous system. Glia. 2001;36:118–24.
10. Norris GT, Kipnis J. Immune cells and CNS physiology: Microglia and beyond. J Exp Med. 2019;216:60–70.
11. Khandelwal PJ, Herman AM, Moussa CE. Inflammation in the early stages of neurodegenerative pathology. J Neuroimmunol. 2011;238:1–11.
12. Prinz M, Priller J, Sisodia SS, Ransohoff RM. Heterogeneity of CNS myeloid cells and their roles in neurodegeneration. Nat Neurosci. 2011;14:1227–35.
13. Ginhoux F, Lim S, Hoeffel G, Low D, Huber T. Origin and differentiation of microglia. Front Cell Neurosci. 2013;7:45.
14. Ajami B, Bennett JL, Krieger C, Tetzlaff W, Rossi FM. Local self-renewal can sustain CNS microglia maintenance and function throughout adult life. Nat Neurosci. 2007;10:1538–43.

15. Huang Y, Xu Z, Xiong S, Sun F, Qin G, Hu G, et al. Repopulated microglia are solely derived from the proliferation of residual microglia after acute depletion. Nat Neurosci. 2018;21:530–40.
16. Nimmerjahn A, Kirchhoff F, Helmchen F. Resting microglial cells are highly dynamic surveillants of brain parenchyma in vivo. Science. 2005;308:1314–8.
17. Olah M, Biber K, Vinet J, Boddeke HW. Microglia phenotype diversity. CNS Neurol Disord Drug Targets. 2011;10:108–18.
18. Baron R, Babcock AA, Nemirovsky A, Finsen B, Monsonego A. Accelerated microglial pathology is associated with Abeta plaques in mouse models of Alzheimer's disease. Aging Cell. 2014;13:584–95.
19. Sierra A, Gottfried-Blackmore AC, McEwen BS, Bulloch K. Microglia derived from aging mice exhibit an altered inflammatory profile. Glia. 2007;55:412–24.
20. Akiguchi I, Pallas M, Budka H, Akiyama H, Ueno M, Han J, et al. SAMP8 mice as a neuropathological model of accelerated brain aging and dementia: Toshio Takeda's legacy and future directions. Neuropathology. 2017;37:293–305.
21. Morley JE, Farr SA, Kumar VB, Armbrecht HJ. The SAMP8 mouse: a model to develop therapeutic interventions for Alzheimer's disease. Curr Pharm Des. 2012;18:1123–30.
22. Perry VH, Nicoll JA, Holmes C. Microglia in neurodegenerative disease. Nat Rev Neurol. 2010;6:193–201.
23. Kim YS, Joh TH. Microglia, major player in the brain inflammation: their roles in the pathogenesis of Parkinson's disease. Exp Mol Med. 2006;38:333–47.
24. Tao Q, Ang TFA, DeCarli C, Auerbach SH, Devine S, Stein TD, et al. Association of Chronic Low-grade Inflammation With Risk of Alzheimer Disease in ApoE4 Carriers. JAMA Netw Open. 2018;1:e183597.
25. Carroll JC, Iba M, Bangasser DA, Valentino RJ, James MJ, Brunden KR, et al. Chronic stress exacerbates tau pathology, neurodegeneration, and cognitive performance through a corticotropin-releasing factor receptor-dependent mechanism in a transgenic mouse model of tauopathy. J Neurosci. 2011;31:14436–49.
26. Tran TT, Srivareerat M, Alkadhi KA. Chronic psychosocial stress triggers cognitive impairment in a novel at-risk model of Alzheimer's disease. Neurobiol Dis. 2010;37:756–63.
27. Gotz J, Bodea LG, Goedert M. Rodent models for Alzheimer disease. Nat Rev Neurosci. 2018;19:583–98.
28. Morley JE. The SAMP8 mouse: a model of Alzheimer. disease? Biogerontology. 2002;3:57–60.
29. Pallas M, Camins A, Smith MA, Perry G, Lee HG, Casadesus G. From aging to Alzheimer's disease: unveiling "the switch" with the senescence-accelerated mouse model (SAMP8). J Alzheimers Dis. 2008;15:615–24.
30. Takeda T. Senescence-accelerated mouse (SAM) with special references to neurodegeneration models, SAMP8 and SAMP10 mice. Neurochem Res. 2009;34:639–59.
31. Miyamoto M. Characteristics of age-related behavioral changes in senescence-accelerated mouse SAMP8 and SAMP10. Exp Gerontol. 1997;32:139–48.

32. Yagi H, Irino M, Matsushita T, Katoh S, Umezawa M, Tsuboyama T, et al. Spontaneous spongy degeneration of the brain stem in SAM-P/8 mice, a newly developed memory-deficient strain. J Neuropathol Exp Neurol. 1989;48:577–90.
33. Kawamata T, Akiguchi I, Yagi H, Irino M, Sugiyama H, Akiyama H, et al. Neuropathological studies on strains of senescence-accelerated mice (SAM) with age-related deficits in learning and memory. Exp Gerontol. 1997;32:161–9.
34. Nomura Y, Okuma Y. Age-related defects in lifespan and learning ability in SAMP8 mice. Neurobiol Aging. 1999;20:111–5.
35. Spangler EL, Patel N, Speer D, Hyman M, Hengemihle J, Markowska A, et al. Passive avoidance and complex maze learning in the senescence accelerated mouse (SAM): age and strain comparisons of SAM P8 and R1. J Gerontol A Biol Sci Med Sci. 2002;57:B61–8.
36. Diaz-Moreno M, Hortiguela R, Goncalves A, Garcia-Carpio I, Manich G, Garcia-Bermudez E, et al. Abeta increases neural stem cell activity in senescence-accelerated SAMP8 mice. Neurobiol Aging. 2013;34:2623–38.
37. Diaz-Moreno M, Armenteros T, Gradari S, Hortiguela R, Garcia-Corzo L, Fontan-Lozano A, et al. Noggin rescues age-related stem cell loss in the brain of senescent mice with neurodegenerative pathology. Proc Natl Acad Sci U S A. 2018;115:11625–30.
38. Mrak RE. Microglia in Alzheimer brain: a neuropathological perspective. Int J Alzheimers Dis. 2012;2012:165021.
39. Fuster-Matanzo A, Llorens-Martin M, Hernandez F, Avila J. Role of neuroinflammation in adult neurogenesis and Alzheimer disease: therapeutic approaches. Mediators Inflamm. 2013;2013:260925.
40. Bayram B, Nikolai S, Huebbe P, Ozcelik B, Grimm S, Grune T, et al. Biomarkers of oxidative stress, antioxidant defence and inflammation are altered in the senescence-accelerated mouse prone 8. Age (Dordr). 2013;35:1205–17.
41. Grinan-Ferre C, Palomera-Avalos V, Puigoriol-Illamola D, Camins A, Porquet D, Pla V, et al. Behaviour and cognitive changes correlated with hippocampal neuroinflammaging and neuronal markers in female SAMP8, a model of accelerated senescence. Exp Gerontol. 2016;80:57–69.
42. Tha KK, Okuma Y, Miyazaki H, Murayama T, Uehara T, Hatakeyama R, et al. Changes in expressions of proinflammatory cytokines IL-1beta, TNF-alpha and IL-6 in the brain of senescence accelerated mouse (SAM) P8. Brain Res. 2000;885:25–31.
43. Shaftel SS, Griffin WS, O'Banion MK. The role of interleukin-1 in neuroinflammation and Alzheimer disease: an evolving perspective. J Neuroinflammation. 2008;5:7.
44. Ye SM, Johnson RW. Increased interleukin-6 expression by microglia from brain of aged mice. J Neuroimmunol. 1999;93:139–48.
45. Heppner FL, Ransohoff RM, Becher B. Immune attack: the role of inflammation in Alzheimer disease. Nat Rev Neurosci. 2015;16:358–72.

46. Niraula A, Sheridan JF, Godbout JP. Microglia Priming with Aging and Stress. Neuropsychopharmacology. 2017;42:318–33.
47. Perry VH, Teeling J. Microglia and macrophages of the central nervous system: the contribution of microglia priming and systemic inflammation to chronic neurodegeneration. Semin Immunopathol. 2013;35:601–12.
48. Neher JJ, Cunningham C. Priming Microglia for Innate Immune Memory in the Brain. Trends Immunol. 2019;40:358–74.
49. Cunningham C, Campion S, Lunnon K, Murray CL, Woods JF, Deacon RM, et al. Systemic inflammation induces acute behavioral and cognitive changes and accelerates neurodegenerative disease. Biol Psychiatry. 2009;65:304–12.
50. Morris MC, Gilliam EA, Button J, Li L. Dynamic modulation of innate immune response by varying dosages of lipopolysaccharide (LPS) in human monocytic cells. J Biol Chem. 2014;289:21584–90.
51. Bartolome F, de la Cueva M, Pascual C, Antequera D, Fernandez T, Gil C, et al. Amyloid beta-induced impairments on mitochondrial dynamics, hippocampal neurogenesis, and memory are restored by phosphodiesterase 7 inhibition. Alzheimers Res Ther. 2018;10:24.
52. Quintana E, Fernandez A, Velasco P, de AB, Liste, Sancho I. D et al. DNGR-1(+) dendritic cells are located in meningeal membrane and choroid plexus of the noninjured brain. Glia. 2015;63:2231–48.
53. Catalin B, Mitran S, Albu C, Iancau M. Comparative aspects of microglia reaction in white and gray matter. Curr Health Sci J. 2013;39:151–4.
54. Ferreira T, Ou Y, Li S, Giniger E, van Meyel DJ. Dendrite architecture organized by transcriptional control of the F-actin nucleator Spire. Development. 2014;141:650–60.
55. Ristanovic D, Milosevic NT, Stulic V. Application of modified Sholl analysis to neuronal dendritic arborization of the cat spinal cord. J Neurosci Methods. 2006;158:212–8.
56. Carson MJ, Reilly CR, Sutcliffe JG, Lo D. Mature microglia resemble immature antigen-presenting cells. Glia. 1998;22:72–85.
57. Auge E, Cabezon I, Pelegri C, Vilaplana J. New perspectives on corpora amylacea in the human brain. Sci Rep. 2017;7:41807.
58. Akiyama H, Kameyama M, Akiguchi I, Sugiyama H, Kawamata T, Fukuyama H, et al. Periodic acid-Schiff (PAS)-positive, granular structures increase in the brain of senescence accelerated mouse (SAM). Acta Neuropathol. 1986;72:124–9.
59. Manich G, Cabezon I, Auge E, Pelegri C, Vilaplana J. Periodic acid-Schiff granules in the brain of aged mice: From amyloid aggregates to degenerative structures containing neo-epitopes. Ageing Res Rev. 2016;27:42–55.
60. Nakamura S, Akiguchi I, Seriu N, Ohnishi K, Takemura M, Ueno M, et al. Monoamine oxidase-B-positive granular structures in the hippocampus of aged senescence-accelerated mouse (SAMP8). Acta Neuropathol. 1995;90:626–32.

61. Schoenen J. The dendritic organization of the human spinal cord: the dorsal horn. Neuroscience. 1982;7:2057–87.
62. Garcia-Segura LM, Perez-Marquez J. A new mathematical function to evaluate neuronal morphology using the Sholl analysis. J Neurosci Methods. 2014;226:103–9.
63. Tremblay ME, Zettel ML, Ison JR, Allen PD, Majewska AK. Effects of aging and sensory loss on glial cells in mouse visual and auditory cortices. Glia. 2012;60:541–58.
64. Hasegawa-Ishii S, Takei S, Chiba Y, Furukawa A, Umegaki H, Iguchi A, et al. Morphological impairments in microglia precede age-related neuronal degeneration in senescence-accelerated mice. Neuropathology. 2011;31:20–8.
65. Paasila PJ, Davies DS, Kril JJ, Goldsbury C, Sutherland GT. The relationship between the morphological subtypes of microglia and Alzheimer's disease neuropathology. Brain Pathol. 2019;29:726–40.
66. Mah LJ, El-Osta A, Karagiannis TC. GammaH2AX as a molecular marker of aging and disease. Epigenetics. 2010;5:129–36.
67. Pospelova TV, Demidenko ZN, Bukreeva EI, Pospelov VA, Gudkov AV, Blagosklonny MV. Pseudo-DNA damage response in senescent cells. Cell Cycle. 2009;8:4112–8.
68. Wyss-Coray T, Mucke L. Inflammation in neurodegenerative disease–a double-edged sword. Neuron. 2002;35:419–32.
69. Hart AD, Wyttenbach A, Perry VH, Teeling JL. Age related changes in microglial phenotype vary between CNS regions: grey versus white matter differences. Brain Behav Immun. 2012;26:754–65.
70. Kawamata T, Akiguchi I, Maeda K, Tanaka C, Higuchi K, Hosokawa M, et al. Age-related changes in the brains of senescence-accelerated mice (SAM): association with glial and endothelial reactions. Microsc Res Tech. 1998;43:59–67.
71. Jung S, Aliberti J, Graemmel P, Sunshine MJ, Kreutzberg GW, Sher A, et al. Analysis of fractalkine receptor CX(3)CR1 function by targeted deletion and green fluorescent protein reporter gene insertion. Mol Cell Biol. 2000;20:4106–14.
72. Ransohoff RM, Engelhardt B. The anatomical and cellular basis of immune surveillance in the central nervous system. Nat Rev Immunol. 2012;12:623–35.
73. Pelegri C, Canudas AM, del VJ, Casadesus, Smith G, Camins MA. A et al. Increased permeability of blood-brain barrier on the hippocampus of a murine model of senescence. Mech Ageing Dev. 2007;128:522–8.
74. Ford AL, Goodsall AL, Hickey WF, Sedgwick JD. Normal adult ramified microglia separated from other central nervous system macrophages by flow cytometric sorting. Phenotypic differences defined and direct ex vivo antigen presentation to myelin basic protein-reactive CD4 + T cells compared. J Immunol. 1995;154:4309–21.
75. Baron JL, Madri JA, Ruddle NH, Hashim G, Janeway CA. Jr. Surface expression of alpha 4 integrin by CD4 T cells is required for their entry into brain parenchyma. J Exp Med. 1993;177:57–68.

76. Engelhardt B, Sorokin L. The blood-brain and the blood-cerebrospinal fluid barriers: function and dysfunction. Semin Immunopathol. 2009;31:497–511.
77. Bowman RL, Klemm F, Akkari L, Pyonteck SM, Sevenich L, Quail DF, et al. Macrophage Ontogeny Underlies Differences in Tumor-Specific Education in Brain Malignancies. Cell Rep. 2016;17:2445–59.
78. Lucin KM, Wyss-Coray T. Immune activation in brain aging and neurodegeneration: too much or too. little? Neuron. 2009;64:110–22.
79. Chen Z, Jalabi W, Shpargel KB, Farabaugh KT, Dutta R, Yin X, et al. Lipopolysaccharide-induced microglial activation and neuroprotection against experimental brain injury is independent of hematogenous TLR4. J Neurosci. 2012;32:11706–15.
80. Furube E, Kawai S, Inagaki H, Takagi S, Miyata S. Brain Region-dependent Heterogeneity and Dose-dependent Difference in Transient Microglia Population Increase during Lipopolysaccharide-induced Inflammation. Sci Rep. 2018;8:2203.
81. Perry VH, Newman TA, Cunningham C. The impact of systemic infection on the progression of neurodegenerative disease. Nat Rev Neurosci. 2003;4:103–12.
82. Wolozin B. Regulated protein aggregation: stress granules and neurodegeneration. Mol Neurodegener. 2012;7:56.
83. Mouton PR, Long JM, Lei DL, Howard V, Jucker M, Calhoun ME, et al. Age and gender effects on microglia and astrocyte numbers in brains of mice. Brain Res. 2002;956:30–5.
84. VanGuilder HD, Bixler GV, Brucklacher RM, Farley JA, Yan H, Warrington JP, et al. Concurrent hippocampal induction of MHC II pathway components and glial activation with advanced aging is not correlated with cognitive impairment. J Neuroinflammation. 2011;8:138.
85. Long JM, Kalehua AN, Muth NJ, Calhoun ME, Jucker M, Hengemihle JM, et al. Stereological analysis of astrocyte and microglia in aging mouse hippocampus. Neurobiol Aging. 1998;19:497–503.
86. Adachi M, Abe M, Sasaki T, Kato H, Kasahara J, Araki T. Role of inducible or neuronal nitric oxide synthase in neurogenesis of the dentate gyrus in aged mice. Metab Brain Dis. 2010;25:419–24.
87. Hayakawa N, Kato H, Araki T. Age-related changes of astorocytes, oligodendrocytes and microglia in the mouse hippocampal CA1 sector. Mech Ageing Dev. 2007;128:311–6.
88. Liu J, Wang MW, Gu P, Ma QY, Wang YY, Geng Y, et al. Microglial activation and age-related dopaminergic neurodegeneration in MPTP-treated SAMP8 mice. Brain Res. 2010;1345:213–20.
89. Matyszak MK, Denis-Donini S, Citterio S, Longhi R, Granucci F, Ricciardi-Castagnoli P. Microglia induce myelin basic protein-specific T cell anergy or T cell activation, according to their state of activation. Eur J Immunol. 1999;29:3063–76.
90. Frank MG, Barrientos RM, Biedenkapp JC, Rudy JW, Watkins LR, Maier SF. mRNA up-regulation of MHC II and pivotal pro-inflammatory genes in normal brain aging. Neurobiol Aging. 2006;27:717–22.
91. Frank MG, Barrientos RM, Watkins LR, Maier SF. Aging sensitizes rapidly isolated hippocampal microglia to LPS ex vivo. J Neuroimmunol. 2010;226:181–4.

92. Perry VH, Matyszak MK, Fearn S. Altered antigen expression of microglia in the aged rodent CNS. Glia. 1993;7:60–7.
93. Vanguilder HD, Bixler GV, Brucklacher RM, Farley JA, Yan H, Warrington JP, et al. Concurrent hippocampal induction of MHC II pathway components and glial activation with advanced aging is not correlated with cognitive impairment. J Neuroinflammation. 2011;8:138.
94. Henry CJ, Huang Y, Wynne AM, Godbout JP. Peripheral lipopolysaccharide (LPS) challenge promotes microglial hyperactivity in aged mice that is associated with exaggerated induction of both pro-inflammatory IL-1beta and anti-inflammatory IL-10 cytokines. Brain Behav Immun. 2009;23:309–17.
95. Shimada A, Hasegawa-Ishii S. Senescence-accelerated Mice (SAMs) as a Model for Brain Aging and Immunosenescence. Aging Dis. 2011;2:414–35.
96. Lee JK, Tansey MG. Microglia isolation from adult mouse brain. Methods Mol Biol. 2013;1041:17–23.
97. Sedgwick JD, Schwender S, Imrich H, Dorries R, Butcher GW. ter M, V. Isolation and direct characterization of resident microglial cells from the normal and inflamed central nervous system. Proc Natl Acad Sci U S A. 1991;88:7438–42.
98. Legroux L, Pittet CL, Beauseigle D, Deblois G, Prat A, Arbour N. An optimized method to process mouse CNS to simultaneously analyze neural cells and leukocytes by flow cytometry. J Neurosci Methods. 2015;247:23–31.
99. Posel C, Moller K, Boltze J, Wagner DC, Weise G. Isolation and Flow Cytometric Analysis of Immune Cells from the Ischemic Mouse Brain. J Vis Exp 2016:53658.
100. Singh V, Mitra S, Sharma AK, Gera R, Ghosh D. Isolation and characterization of microglia from adult mouse brain: selected applications for ex vivo evaluation of immunotoxicological alterations following in vivo xenobiotic exposure. Chem Res Toxicol. 2014;27:895–903.
101. Cardona AE, Huang D, Sasse ME, Ransohoff RM. Isolation of murine microglial cells for RNA analysis or flow cytometry. Nat Protoc. 2006;1:1947–51.
102. Ueno M, Sakamoto H, Kanenishi K, Onodera M, Akiguchi I, Hosokawa M. Ultrastructural and permeability features of microvessels in the periventricular area of senescence-accelerated mice (SAM). Microsc Res Tech. 2001;53:232–8.
103. Perry VH, Cunningham C, Holmes C. Systemic infections and inflammation affect chronic neurodegeneration. Nat Rev Immunol. 2007;7:161–7.
104. Perry VH. Contribution of systemic inflammation to chronic neurodegeneration. Acta Neuropathol. 2010;120:277–86.
105. Proescholdt MG, Chakravarty S, Foster JA, Foti SB, Briley EM, Herkenham M. Intracerebroventricular but not intravenous interleukin-1beta induces widespread vascular-mediated leukocyte infiltration and immune signal mRNA expression followed by brain-wide glial activation. Neuroscience. 2002;112:731–49.
106. Depino A, Ferrari C, Pott Godoy MC, Tarelli R, Pitossi FJ. Differential effects of interleukin-1beta on neurotoxicity, cytokine induction and glial reaction in specific brain regions. J Neuroimmunol.

2005;168:96–110.
107. Hasegawa-Ishii S, Inaba M, Shimada A. Widespread time-dependent changes in tissue cytokine concentrations in brain regions during the acute phase of endotoxemia in mice. Neurotoxicology. 2020;76:67–74.

Figures

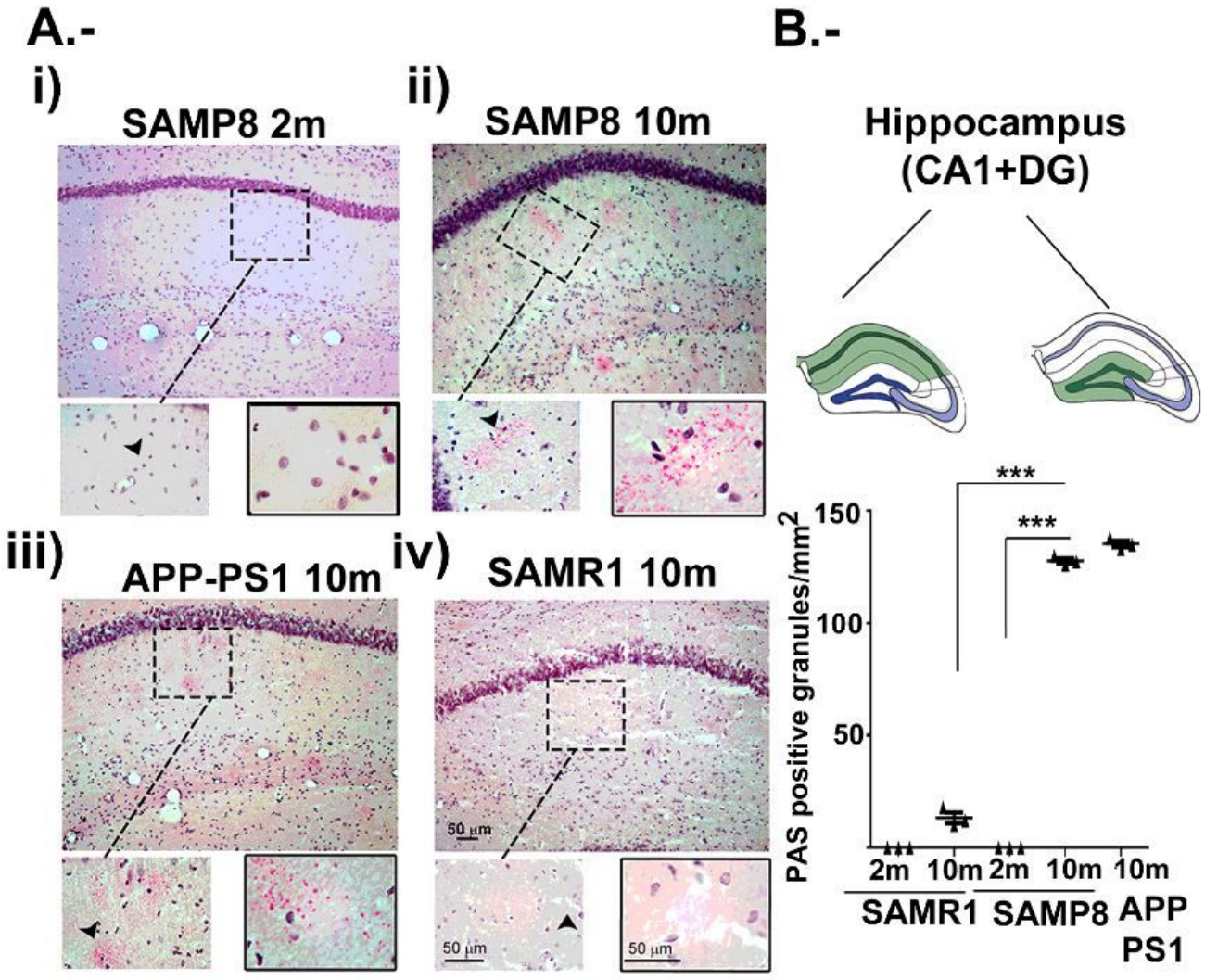

Figure 1

Analysis of PAS accumulations in SAM mice associated with aging and neurodegeneration. (A) Representative captures of hippocampal regions in SAMR1 and SAMP8 mice of 2 and 10 months (m) and 10 m old APP-PS1 mice showing PAS-positive granules. (B) Quantification of PAS positive accumulates. Brain sections were stained by Schiff's reagent (red-pink) and nuclei with hematoxylin (blue-brown). Images of coronal sections of cryostat (30 µm thick) were obtained with a 20X objective

(40x and 100x, from left to right for detail pictures), with the Nikon Eclipse 50i H550S light microscope and processed with the help of the NIS elements of software and ImageJ. ***, p≤ 0.001 and **, p≤ 0.01 with respect to the PAS /mm2 accumulations (n = 3 to 5). Scale bars are included in the images.

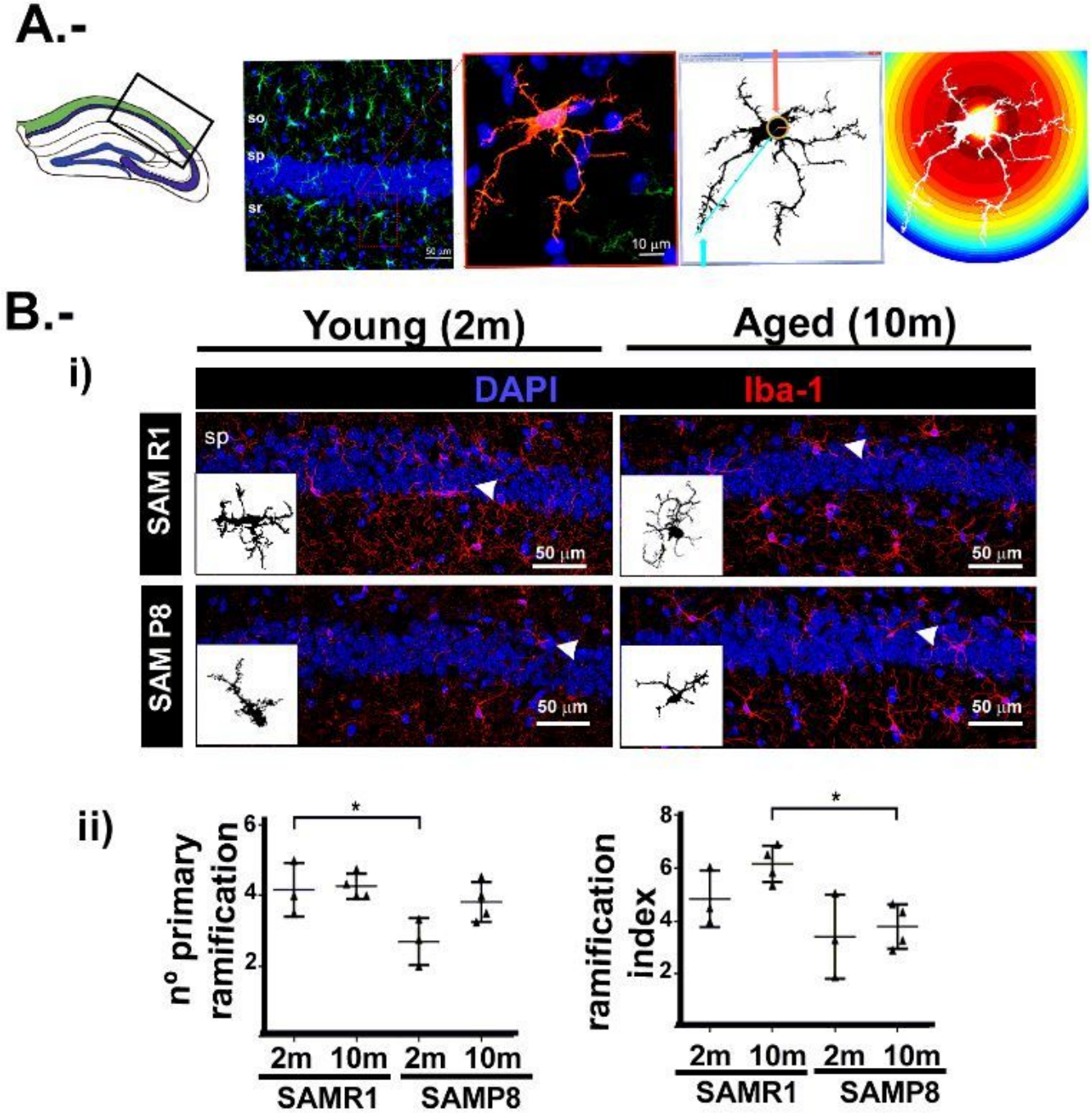

Figure 2

Morphology analysis by Sholl analysis. A.- (i) Representative image of hippocampus Iba1+ (green) regions used for analysis. (ii) Iba1+ maximum projection detailed capture of cell morphology. (iii). Binary image of the maximum projection of the detailed image. Cartoon showing the radius of the longest extension that corresponds to the radius of the largest concentric circle and furthest from the soma (ending radius or maximum radius) and the radius that would cover the soma (starting radius or initial

radius). B.- (i) Representative images of brain maps from 2 m and 10 m SAM hippocampus areas using a 40x objective and 1.7x digital zoom, showing 63x detailed images of iba1+ positive binary image showing cell morphology. (ii) Sholl analysis results, number of primary branches and branch index from iba-1+ of 2 and 10 month old SAM mice hippocampus area (n = 3). Images were obtained with a Leica SP5 TCS inverted fluorescence confocal microscope from cryostat sections 30 µm thick. The nuclei with DAPI (blue); the brain microglia/macrophages are stained with Iba-1. Scale bars are included in the images.

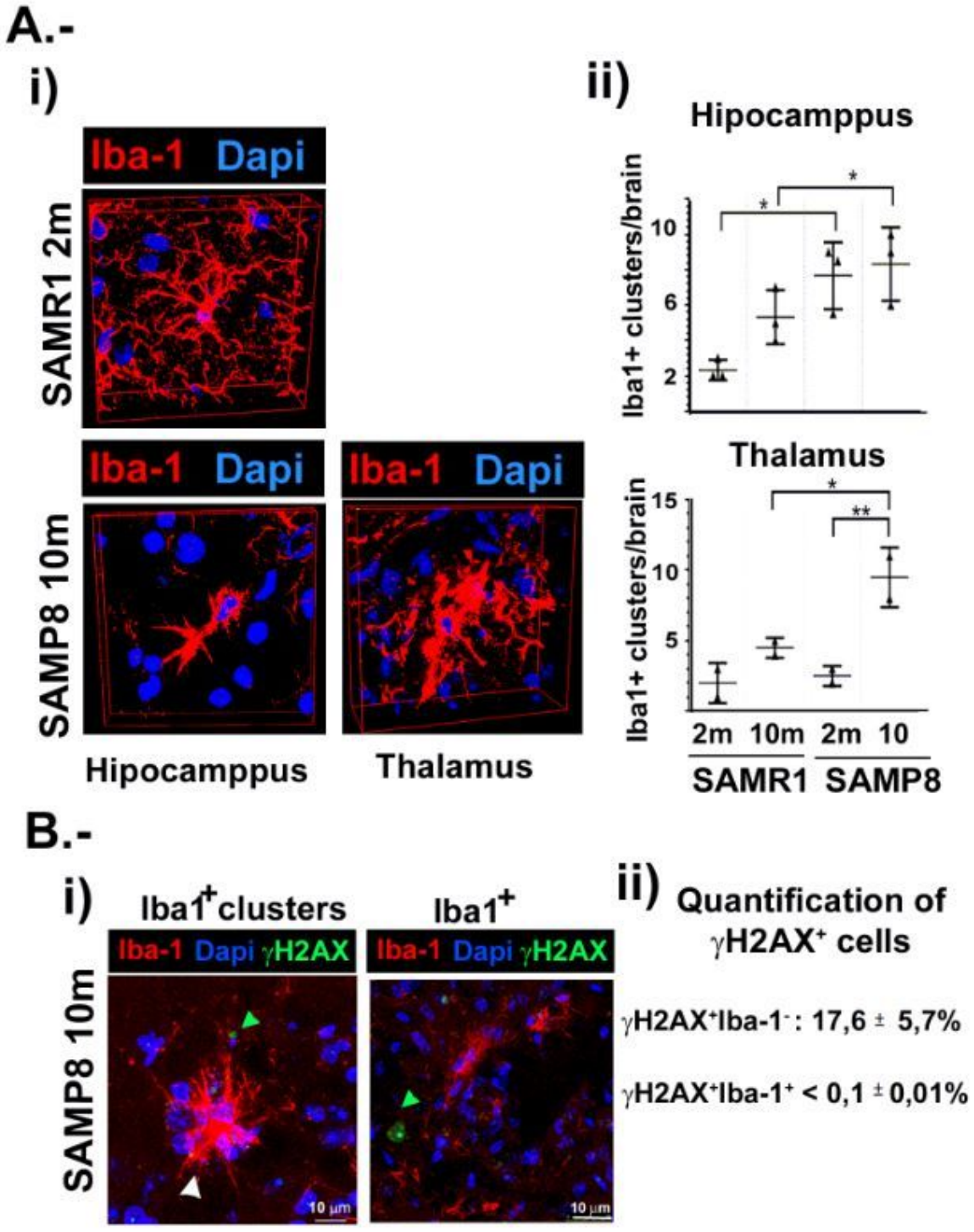

Figure 3

Iba1+ clusters analysis of young and aged SAM mice. 2 and 10 months SAMP8 and SAMR1 brains were stained with Iba-1 for microglia/macrophages (red), γH2AX for DNA damage in green and DAPI for nuclei (blue). Images from Iba1+ stained brains were taken with a 63x objective (3x digital zoom) and processed with ImageJ, using the high-level 3D visualization framework plugin for 3D reconstructions. A.- (i) Representative 3D reconstruction from hippocampus Iba1+ cells of young 2 m SAMR1 animal as control. 10 m SAMP8 Iba1+ from hippocampus and thalamus showing Iba1+ cell clusters. (ii) Quantification of microglia clusters (Iba-1+) in 2 and 10 m old SAMR1 and SAMP8 brain regions indicated. B.- Co-localization of Iba1 immunofluorescence (red) and γH2AX+ (green) in 30 m coronal cryostat sections of 10 m old SAMP8 brains. (i) Representative image of maximum projection of 10 months SAMP8 hippocampus showing microglia Iba-1+ cellular cluster (red), DAPI (blue) and γH2AX+ (green). γH2AX+ cells outside Iba-1+ clusters are marked with a green arrow (ii) Quantification of γH2AX+ cells. γH2AX+ Iba-1- cells are abundant in 10m SAMP8 brains showing specificity of antibody. ***, p≤ 0.001; **, p≤ 0.01 and *, p≤ 0.05 (n = 5) with respect to the number of clusters / mouse brain (n = 5). Scale bars are included in the images. The images are representative of an experiment of n = 3 .

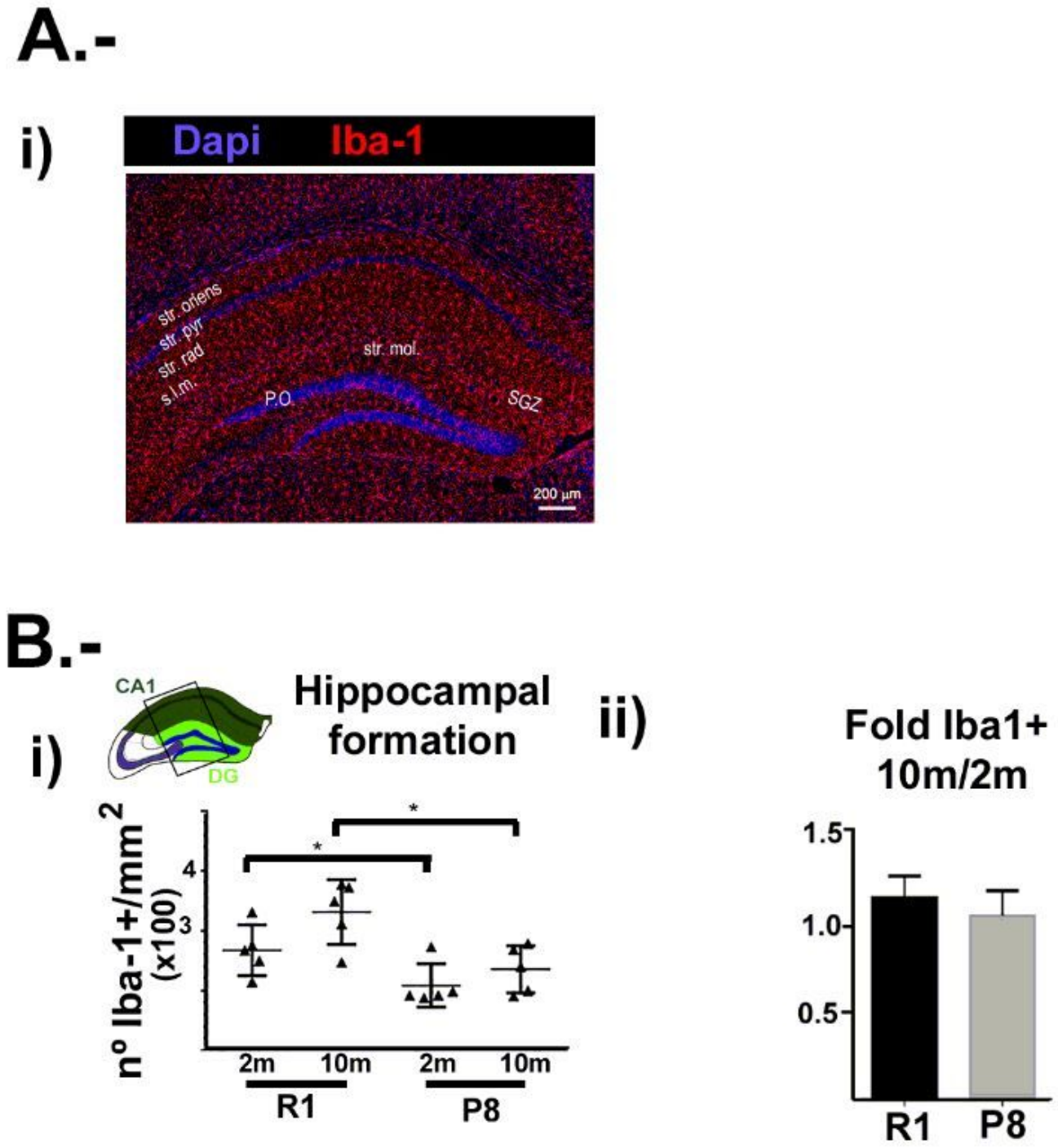

Figure 4

Evaluation of Iba1+ cells in the hippocampus of SAM mice aged 2 and 10 months. 30 µm coronal cryostat sections were stained with Iba-1 (red) and nuclei with DAPI (blue). Images at 40x (1.7x digital zoom) were obtained with a Leica SP5 TCS inverted fluorescence confocal microscope and the areas were processed and evaluated with ImageJ. (A) Representative map of the hippocampus (Hpp) (i), showing the expression of BP myeloid cells Iba1+ in 2 m SAMR1 mice and indicating the regions used for counting. (ii) Representative aging phenotype of SAM mice at 10 m, showing incipient alopecia and skin lesions. B.- Hpp area used in the quantification of Iba-1+ are surrounded by a box, differing in CA1 (cornus

ammonis) in dark green and DG (dentate gyrus) soft green, as shown in the scheme. Quantification of Iba1+ cells in the area described in 2 m and 10 m SAM mice. (ii) Fold change of Hpp Iba1+ of 10 m versus 2 m in SAMR1 and P8 mice. Scale bars are included in the image. ***, P ≤ 0.001; **, p≤ 0.01 and *, p≤ 0.05 with respect to Iba-1 + / mm2 cells in BP (n = 5).

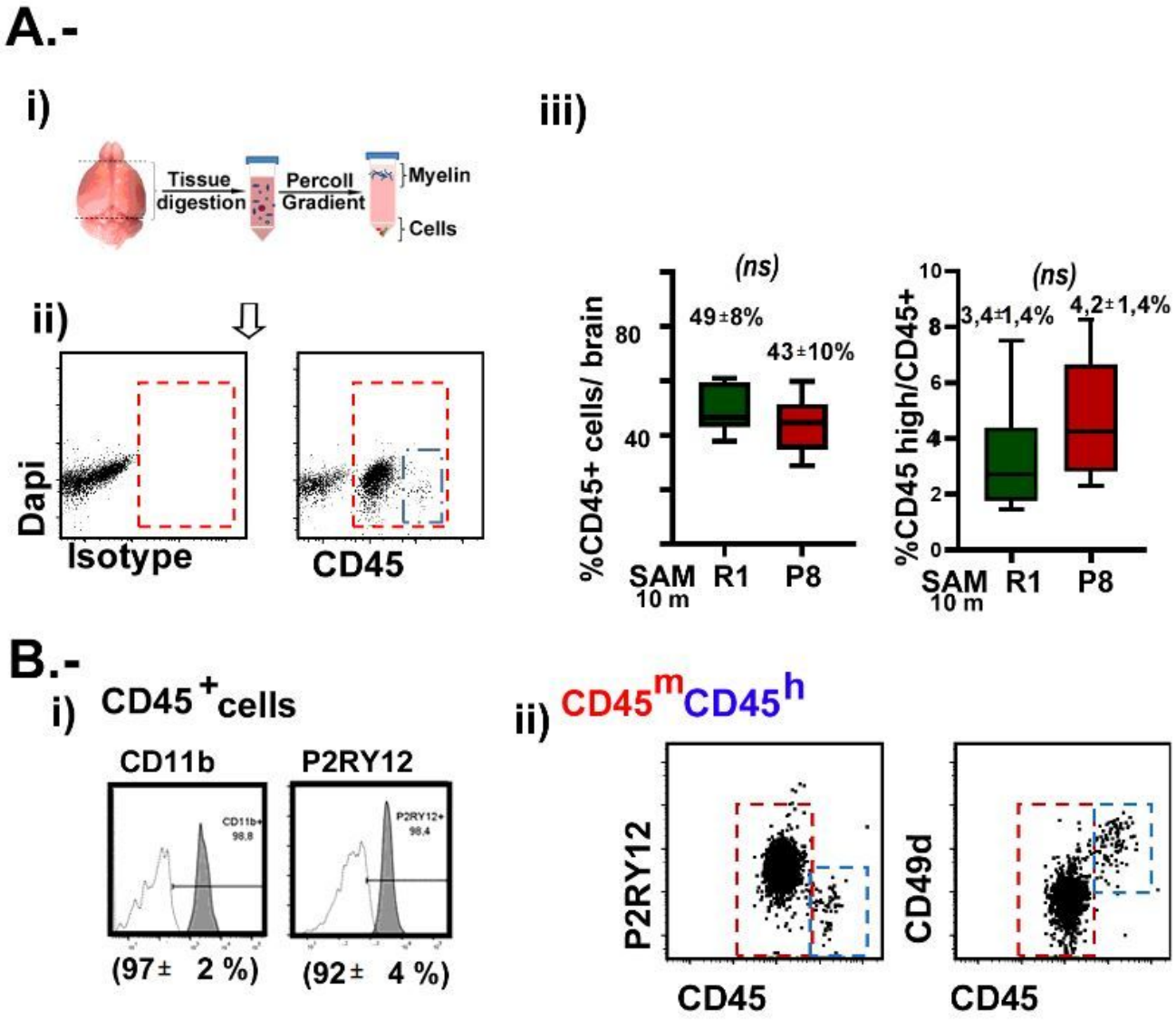

Figure 5

Isolation and quantification of CD45-positive brain cells. A.- (i). Cartoon representing the brain isolation procedure. (ii) Flow cytometry dot plots of live cells isolated from brain except cerebellum and olfactory bulb (OB) and meningeal membranes and choroid plexus. Cells were isolated from 10 m SAM P8 and R1 mice, and stained with control isotype antibody (APC rat IgG2b) or with APC rat anti-mouse CD45. Red box marks CD45 medium expression cells and blue box marks CD45 high expression cells. Panel iii) shows the arithmetic mean ± SEM (n=10) of the percentage of total CD45+ cells isolated in 10 m SAMR1 (green) and SAMP8 (red) brains, and the percentage of cells which express a high expression of CD45. The gating strategy was as presented in additional Fig 2s. B.- (i) Cells were stained with PE-Cy7 rat anti-

mouse CD45 together with 488 rat anti-mouse CD11b and APC rat anti-mouse P2RY12. Representative histograms are shown, displaying the surface staining of CD11b and P2RY12 of BP CD45m cells: white histograms represent isotype control and grey histograms represent specific staining with the antibodies indicated. Numbers inside show that most of the CD45+ cells are CD11b+ and P2RY12+ (n=10). Histograms on the right show staining on the surface of CD11b and P2RY12 of BP CD45m cells: white histograms represent isotype control and grey histograms represent specific staining with the antibodies indicated. (ii) Cells were stained with PE-Cy7 rat anti-mouse CD45 and APC rat anti-mouse P2RY12 or CD49d. CD45m cells were P2RY12+ CD49d- (red box) and CD45h cells were P2RY12- CD49d+ cells (blue box).

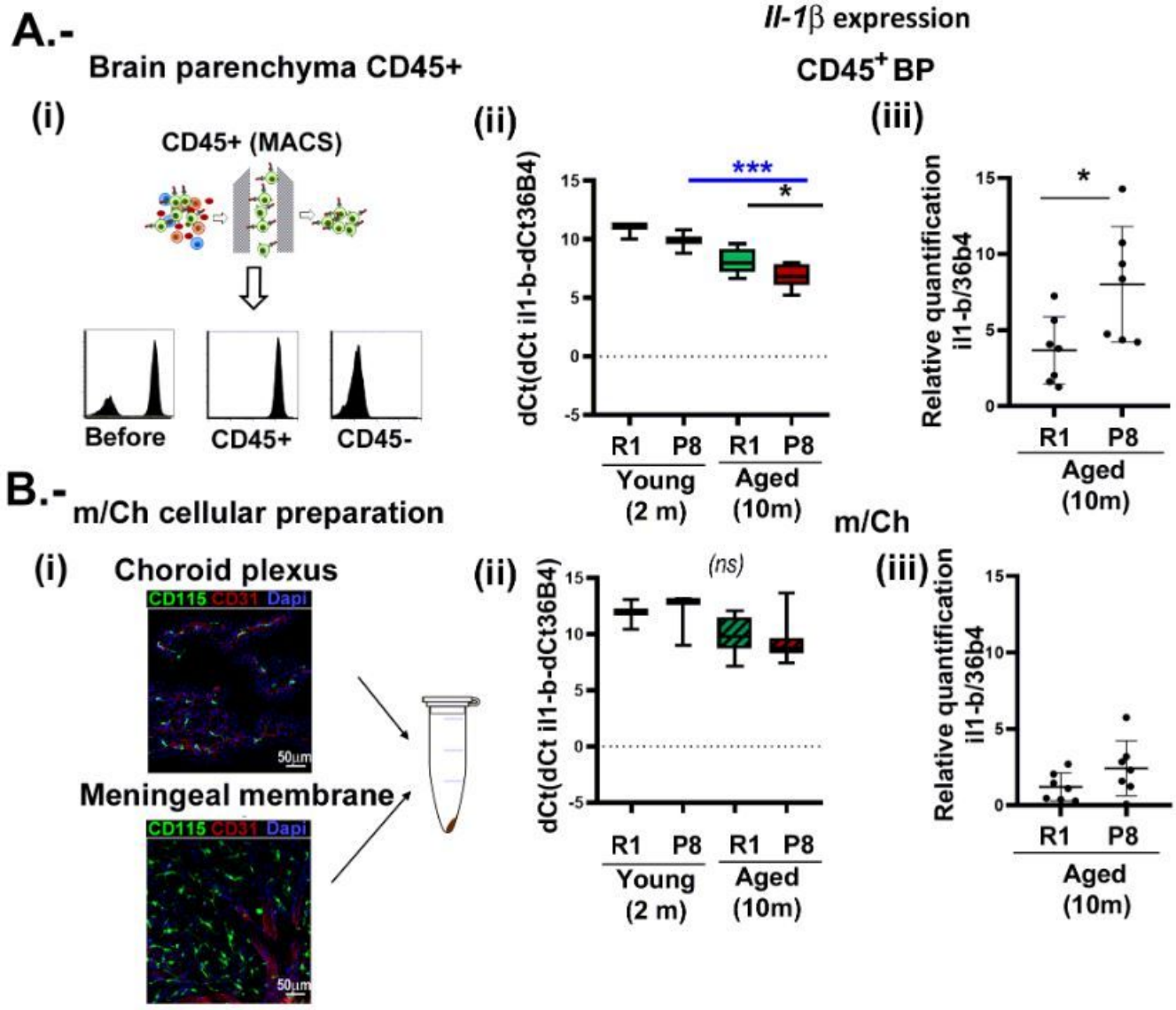

Figure 6

Higher Il-1β expression occurs mainly in aged SAMP8 CD45+ brain parenchymal cells. RT-PCR analysis of IL-1βmRNA expression. A.- CD45+ brain parenchymal (BP) cells. (i) Scheme of BP CD45+ magnetic cell separation and histograms showing CD45 staining by cytometry from CD45+ and CD45- fraction.

Quantification of BP CD45+ obtained in positive fraction was of 97±2 % (arithmetic mean ± SEM (n=5) of CD45+ cell from alive cells as in additional Fig 2s. (ii) IL-1□□□mRNA expression from BP CD45+ isolated from young (2 m) and aged (10 m) SAMP8 (red) and SAMR1 (green) animals. B.- (i) Dissected choroid plexus and meningeal membranes (m/Ch) as in material were pooled into an Eppendorf and total RNA obtained as in material section, We show the abundance of Iba1+ cells (green) by immunofluorescence in both brain localizations which were similar as in [52]. Images were obtained with a SP5 Leica TCS confocal fluorescent microscope. Scale bars are included in the images that are representative of the different brain localizations. (ii) Il-1□□□mRNA expression from m/Ch preparation from young (2 m) and aged (10 m) SAMP8 (red) and SAMR1 (green) animals. Specific mRNAs are amplified from total mRNA using SYBR Green Real time PCR methodology using 36B4 as reference gene. Data are presented as dCt (Ct il1□-Ct 36B4). Lower values of dCt means higher Il1-□ transcript expression in the sample. *** p<0.001 or ** p<0.01 between specified groups.

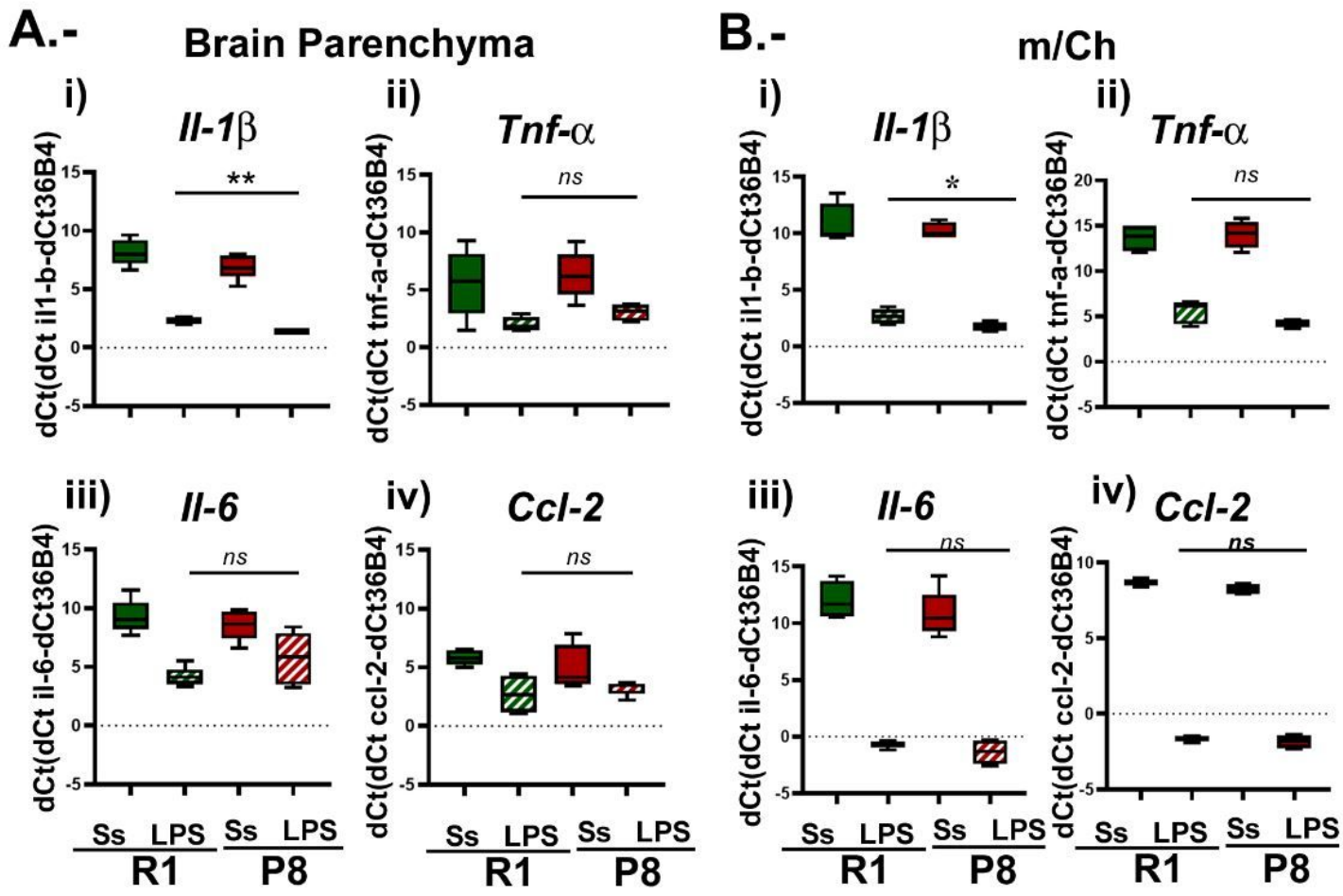

Figure 7

bMyC from brain parenchyma (BP) and m/Ch respond to low doses of systemic LPS. Isolated CD45+ cells form BP and m/Ch preparation as in Fig 6. A.- BP CD45+ B.- m/Ch preparations, from aged (10 m) old SAMR1 (green bars) and SAMP8 (red bars) were injected with saline (empty bars) or LPS (1mg/ml) (stripped bars) for 3 hours and Il1-□□(panel i) Tnf-□□(panel ii), Il-6 (panel iii) and Ccl2 (panel iv) mRNA expression was then quantified by real-time PCR as before. Cytokines mRNAs increased significantly 3 h

after the injection of LPS. Specific mRNAs are amplified from total mRNA using SYBR Green Real time PCR methodology using 36b4 as reference gene. Graphs are presented as dCt (Ct gene-Ct 36b4). Lower values of dCt means higher cytokine transcript expression in the sample. *** $p<0.001$ or ** $p<0.01$ between specified groups.

Supplementary Files

This is a list of supplementary files associated with this preprint. Click to download.

- FigureLegendAdditionalFigs.docx
- AdditionalFigure4S.tif
- AdditionalFigure3S.tif
- AdditionalFigure2S.tif
- AdditionalFigure1S.tif